Nanoscale

ROYAL SOCIETY OF CHEMISTRY

PAPER

View Article Online
View Journal | View Issue

Cite this: *Nanoscale*, 2023, **15**, 4488

Self-assembled three-dimensional hydrogels based on graphene derivatives and cerium oxide nanoparticles: scaffolds for co-culture of oligodendrocytes and neurons derived from neural stem cells†

Yurena Polo, [a] Jon Luzuriaga, [b] Sergio Gonzalez de Langarica, [c] Beatriz Pardo-Rodríguez, [b] Daniel E. Martínez-Tong, [d] Christos Tapeinos, [e,f] Irene Manero-Roig, [b,g] Edurne Marin, [c] Jone Muñoz-Ugartemendia, [c] Gianni Ciofani, [e] Gaskon Ibarretxe, [b] Fernando Unda, [b] Jose-Ramon Sarasua, [c] Jose Ramon Pineda *[b,h] and Aitor Larrañaga *[c]

Stem cell-based therapies have shown promising results for the regeneration of the nervous system. However, the survival and integration of the stem cells in the neural circuitry is suboptimal and might compromise the therapeutic outcomes of this approach. The development of functional scaffolds capable of actively interacting with stem cells may overcome the current limitations of stem cell-based therapies. In this study, three-dimensional hydrogels based on graphene derivatives and cerium oxide (CeO_2) nanoparticles are presented as prospective supports allowing neural stem cell adhesion, migration and differentiation. The morphological, mechanical and electrical properties of the resulting hydrogels can be finely tuned by controlling several parameters of the self-assembly of graphene oxide sheets, namely the amount of incorporated reducing agent (ascorbic acid) and CeO_2 nanoparticles. The intrinsic properties of the hydrogels, as well as the presence of CeO_2 nanoparticles, clearly influence the cell fate. Thus, stiffer adhesion substrates promote differentiation to glial cell lineages, while softer substrates enhance mature neuronal differentiation. Remarkably, CeO_2 nanoparticle-containing hydrogels support the differentiation of neural stem cells to neuronal, astroglial and oligodendroglial lineage cells, promoting the *in vitro* generation of nerve tissue grafts that might be employed in neuroregenerative cell therapies.

Received 23rd November 2022,
Accepted 24th January 2023

DOI: 10.1039/d2nr06545b

rsc.li/nanoscale

1. Introduction

Neurological disorders cause death or disability to more than 94 million people worldwide every year and this number is expected to rise to 103 million by 2030.[1,2] Among them, stroke is the main cause of chronic impairment and the third leading cause of mortality worldwide.[3] Stroke, like traumatic injuries, causes the death of the neural tissue in the affected area, but also provokes a dysfunction and secondary apoptotic death of the surrounding cells, inhibiting efficient restoration or functional recovery of the damaged tissue.[3,4] Despite their huge socioeconomic impact, there is no available treatment for these conditions nowadays.[5] Therefore, there is a need to explore new therapies that replace the injured neural network and promote the integration of new neurons and glial cells into the central nervous system (CNS).

Among the different approaches to regenerate the CNS, cell-based therapies, particularly those based on neural stem cells

[a]*Polimerbio, Donostia-San Sebastian, Spain*
[b]*Cell Signaling Lab, Department of Cell Biology and Histology, Faculty of Medicine and Nursing, University of the Basque Country (UPV/EHU), Leioa, Spain. E-mail: joseramon.pinedam@ehu.eus; Tel: +34 946 012 426*
[c]*Group of Science and Engineering of Polymeric Biomaterials (ZIBIO Group), Department of Mining, Metallurgy Engineering and Materials Science, POLYMAT, University of the Basque Country (UPV/EHU), Bilbao, Spain. E-mail: aitor.larranagae@ehu.eus; Tel: +34 946 013 935*
[d]*Polymers and advanced materials: Physics, Chemistry and Technology, University of the Basque Country (UPV/EHU), Donostia-San Sebastian, Spain & Centro de Física de Materiales (UPV/EHU-CSIC), Donostia-San Sebastian, Spain*
[e]*Smart Bio-Interfaces, Istituto Italiano di Tecnologia, Pontedera, PI, Italy*
[f]*Division of Pharmacy and Optometry, School of Health Sciences, Faculty of Biology, Medicine and Health, University of Manchester, Manchester, UK*
[g]*Université de Bordeaux IINS – UMR 5297, Bordeaux, France*
[h]*Achucarro Basque Center for Neuroscience Fundazioa, Leioa, Spain*

† Electronic supplementary information (ESI) available. See DOI: https://doi.org/10.1039/d2nr06545b

(NSCs), offer the most straightforward alternative to reestablish a functional neural network by producing therapeutic factors, promoting the self-restoration of the damaged tissue and ultimately replacing the lost neural cells.[4,6] However, the integration of the cells into the host CNS remains challenging.[7] In this regard, tissue engineering offers the possibility to combine NSCs with scaffolds to enhance cell integration on the damaged area.[6] Within the recently coined field of materiobiology, scaffolds are considered multifunctional devices with the capability to finely tune biological functions.[8] In the particular case of nervous system regeneration, materials based on graphene derivatives have attracted considerable attention[9] thanks to the possibility to create moldable platforms (*e.g.*, with tailored chemical, mechanical and electrical features) to promote the adhesion and differentiation of NSCs towards functional glial and neuronal lineages.[10,11] Graphene consists of a single layer of carbon atoms organized in a honeycomb lattice monolayer that can be arranged either in two- (2D) or three-dimensional (3D) scaffolds, thus resembling the complex architecture of the extracellular matrix.[12,13] Although most of the studies with NSCs have been performed in 2D graphene derivative-based scaffolds, recently, 3D scaffolds have been reported to better promote the proliferative ability of NSCs, while maintaining similar adhesion features.[14] Moreover, the physical properties of these 3D scaffolds including stiffness or pore geometry can modulate the adhesion, proliferation and differentiation capabilities of the NSCs.[13] Understanding how these features interact in the formation of complex neural networks that support mature neuronal and glial interplay will be vital to ensure the successful integration of the NSCs into the graphene derivative-based 3D scaffolds.

Three-dimensional composite scaffolds offer several benefits concerning single material scaffolds since they allow a simple modulation of their physicochemical, mechanical and electrical properties by simply modifying their composition while exploiting potential synergistic effects among their constituents.[15] Herein, the combination of 3D scaffolds made of graphene-derivatives and cerium oxide (CeO_2) nanoparticles will be explored as a platform for the regeneration of the CNS. CeO_2 nanoparticles comprise a cubic fluorite arrangement that acts as redox reaction sites thanks to the oxygen deficiencies at the nanoscale order.[16] This oxygen deprivation endows antioxidant features to the CeO_2 nanoparticles that resemble the activity of antioxidant natural enzymes (*i.e.*, superoxide dismutase (SOD) and catalase (CAT)), which is beneficial for the promotion of the angiogenesis and the restoration of the neural architecture.[17,18] Accordingly, CeO_2 nanoparticles have been reported to provide neuroprotective effects, as demonstrated on an adult spinal cord neuron model[19] and *in vivo* on a pharmacologically induced brain oxidative stress model.[20]

In this study, we combine the potential of graphene-based materials to promote the adhesion, proliferation and differentiation of NSCs, with the additional antioxidant and neuroprotective effects associated with CeO_2 nanoparticles as a prospective approach for the restoration of the injured CNS. To achieve this aim, we engineered and characterized 3D hydrogels based on the combination of graphene derivatives and CeO_2 nanoparticles with tunable stiffness, porous geometry and electrical conductivity. We further studied the adhesion, integration and differentiation capabilities of the NSCs towards neuronal, astroglial, and oligodendroglial lineages at different time points. This allowed us to establish heterocellular cultures for *in vitro* studies that mimicked the *in vivo* CNS tissue architecture.

2. Materials and methods

2.1. Fabrication of the hydrogels

Graphene oxide (GO) solution (4 mg ml^{-1} aqueous dispersion from Graphenea, Spain) was pre-diluted with distilled water to a concentration of 2 mg ml^{-1} and sonicated for 30 min. Cerium oxide (CeO_2) nanoparticles (246 mg ml^{-1}, cerium(IV) oxide, 20% in water from Thermo Fisher Scientific, USA) were also sonicated for 30 min to ensure a homogeneous dispersion. For those hydrogels containing CeO_2 nanoparticles, the two dispersions were mixed in the corresponding GO : CeO_2 weight ratios (10 : 0.25; 10 : 0.5; 10 : 0.6; 10 : 0.75 or 10 : 1) and the mixture was then incubated under magnetic stirring for 3 h at 90 °C to facilitate the electrostatic interactions between the negatively charged GO sheets and the positively charged CeO_2 nanoparticles. Samples containing only GO were also treated for 3 h at 90 °C to ensure equal thermal treatment in all the samples. Afterwards, L-ascorbic acid (AsA) (Sigma Aldrich, Spain) was added to reduce the GO sheets and enable hydrogel formation. The corresponding GO : AsA weight ratio (1 : 1; 1 : 4; 1 : 10) was mixed for 30 min under stirring and the self-assembly of the GO was promoted by incubating the solution at 60 °C overnight. The medium of the resulting hydrogels was replaced with distilled water every 12 h for 7 days to ensure the complete elimination of the unreacted AsA. Hydrogels either were lyophilized for characterization or sterilized with 70% ethanol every 12 h for five times. Sterilized hydrogels were washed with sterile phosphate buffered saline (PBS) every 12 h for four times and finally replaced by Neurocult basal medium (STEMCELL Technologies, Canada) one day prior to cell culture experiments.

2.2. Physico-chemical and functional characterization

2.2.1. Transmission electron microscopy (TEM). The successful decoration of the GO sheets with CeO_2 nanoparticles was studied with TEM. Either a previously sonicated dispersion of GO (2 mg ml^{-1}) alone or together with CeO_2 nanoparticles was incubated for 3 h at 90 °C under constant magnetic stirring. Afterwards, the aqueous solution containing either GO sheets, CeO_2 nanoparticles, or GO sheets decorated with CeO_2 nanoparticles was deposited onto carbon-coated grids and imaged in a JEOL 1400 Plus transmission electron microscope (JEOL, Tokyo, Japan).

2.2.2. X-ray diffraction (XRD). The X-ray powder diffraction patterns of the previously lyophilized hydrogels were collected

by using a Philips X'pert PRO automatic diffractometer (Malvern Panalyticals, Malvern, UK) operating at 40 kV and 40 mA, in theta-theta configuration, secondary monochromator with Cu-Kα radiation (λ = 1.5418 Å) and a PIXcel solid state detector (active length in 2θ equal to 3.347°). Data were collected at a 2θ from 5 to 60°, step size equal to 0.026° and time per step of 600 s at room temperature (RT) (total time: 1 h). 1° fixed soller and divergence slit giving a constant volume of sample illumination were used.

2.2.3. Energy-dispersive X-ray spectrometry (EDX). The elemental analysis (spectra and mapping) of the previously lyophilized graphene-based hydrogels containing increasing amounts of CeO_2 nanoparticles was performed using a built-in Bruker Nano XFlash 5010 detector (Bruker, Coventry, UK). Before analysis, the samples were placed on a dual-side conductive carbon tape and were coated with gold at 25 mA for 70 s.

2.2.4. Raman spectroscopy. Raman spectroscopy was performed on the previously lyophilized graphene-based hydrogels containing increasing amounts of CeO_2 nanoparticles using a Horiba LabRAM HR Evolution Raman microscope (Horiba, Kyoto, Japan). The laser excitation wavelength was 532 nm and the scanning range was set from 400 to 3000 cm^{-1}. The samples were placed on top of a silicon wafer and the analysis was performed in at least three random areas of the sample to ensure its homogeneity. The mean values are represented in the graph.

2.2.5. Scanning electron microscopy (SEM). Previously lyophilized hydrogels were directly observed (*i.e.*, without gold or carbon coating) in a scanning electron microscope Hitachi S-3400 N (Hitachi, Tokio, Japan). The pore size of the hydrogels was estimated by using ImageJ v1.53s software (Wayne Rasband & contributors, National Institute of Health, USA).

2.2.6. Rheology. The mechanical properties of the hydrogels were studied applying a torque of 5 μN m, at room temperature and in a range of frequencies from 0.1 to 10 rad s^{-1} in the linear viscoelastic region (LVR) using a TA instruments AR G2 rheometer (TA Instruments, New Castle, USA).

2.2.7. Electrical conductivity. Conductivity measurements were carried out using a Novocontrol Alpha impedance analyzer (Novocontrol Technologies GmbH, Montabaur, Germany). The previously lyophilized hydrogels were pressed between gold electrodes, and an AC electric field was applied (1.5 VRMS, frequency range 1 Hz to 1 MHz). All measurements were performed at room conditions (22 °C, 50 RH%).

2.2.8. Antioxidant capabilities. The antioxidant capacity of the hydrogels decorated with increasing amounts of CeO_2 nanoparticles was determined using Fluorimetric Hydrogen Peroxide Assay Kit (cat# MAK165-1KT, Sigma Aldrich, Spain). Briefly, each hydrogel was exposed to 50 μM hydrogen peroxide solution for 30 min. Thereafter, 50 μL of the medium were placed in a 96-well plate and mixed with 50 μl of the horseradish peroxidase and red peroxidase substrate Mastermix solution. After 20 min of incubation, fluorescence intensity (λ_{ex} = 540 nm/λ_{em} = 590 nm) was measured using a Biotek Synergy H1M microplate reader (Agilent, Santa Clara, CA, USA) to determine the remaining hydrogen peroxide concentration.

2.2.9. X-ray photoelectron spectroscopy (XPS). Previously lyophilized graphene-based hydrogels, the original graphene oxide and graphite (as a control), were subjected to XPS analysis with a SPECS (Germany) instrument equipped with Phoibos 150 1D-DLD analyzer and monochromatized Al Kα (1486.6 eV) radiation source. Survey scans (1100 to 0 eV binding energy, BE; step energy 1 eV; dwell time 0.1 s; pass energy 40 eV) were acquired with an electron take-off angle of 90°. High-resolution scans (step energy 0.1 eV; dwell time 0.1 s; pass energy 30 eV) were also acquired with an electron take-off angle of 90°. The hydrocarbon peak component in the C 1s spectra was set at 285.0 eV to correct sample charging. The spectrometer was previously calibrated with the peak of Ag 3d 5/2 (368.28 eV).

2.2.10. Surface charge of GO and CeO_2 nanoparticles. GO and CeO_2 nanoparticles were thoroughly washed with distilled water and resuspended in a 5 mM NaCl aqueous solution for ζ-potential determination measuring a minimum of ten runs with a Malvern Instrument Zetasizer (ZEN 3690, Malvern, UK).

2.3. Cell culture

2.3.1. Seeding and induction of cell differentiation. Mouse neural stem cells (NSCs) were collected, passaged and seeded in NeuroCult™ proliferation medium as previously described.[11] To compare the effect of the morphology, mechanical properties and electrical conductivity, hydrogels containing the same proportion of GO : AsA (GO : AsA 1 : 1) and four times more AsA (GO : AsA 1 : 4) were selected for cell experiments. The effect of the incorporation of CeO_2 nanoparticles was studied with the GO : AsA 1 : 4 hydrogel containing a proportion of GO : CeO_2 of 10 : 0.25 (GO : AsA 1 : 4 + CeO_2 0.25).

As the hydrogels have different diameters, 60 000 cells were seeded on the GO : AsA 1 : 1 and 30 000 cells were seeded on the GO : AsA 1 : 4 and GO : AsA 1 : 4 + CeO_2 0.25 hydrogels to keep a similar cell density. After 24 h, medium was changed to NeuroCult™ differentiation medium and cells were cultured as previously described.[11]

2.3.2. Scanning electron microscopy (SEM). To study the attachment of the cells to the hydrogels, NSCs were incubated for 24 h over GO : AsA 1 : 1; GO : AsA 1 : 4 and GO : AsA 1 : 4 + CeO_2 0.25 hydrogels and subsequently fixed for 1 h at room temperature using 2% glutaraldehyde (cat# 50-262-19, Fisher Scientific, Pittsburgh, USA) diluted in 0.1 M cacodylate buffer (cat# C0250, Sigma-Aldrich, Spain). Cacodylate buffer and isosmolar sucrose (cat# S7903, Sigma-Aldrich, Spain) were then used to rinse the fixative solution. The samples were post-fixed for 1 h in the dark using 1% osmium tetraoxide (OsO_4) in cacodylate (cat# O5500, Sigma-Aldrich, Spain). Then, OsO_4 was eliminated by rinsing for 10 min each hydrogel with cacodylate buffer. Hydrogels were dehydrated with increasing series of EtOH (30°, 50°, 70°, 90°, 96°, 100°, and 2 × 100° absolute) for 20 min each and air dried for 5 h. Afterwards, conductive cement was used to mount the hydrogels on the scanning elec-

tron microscope supports. Finally, gold nanoparticles were flashed in an argon environment to create a metallic coating. Samples were observed using a Hitachi S-3400 N scanning electron microscope (Hitachi, Tokio, Japan).

2.3.3. Immunostaining. NSCs were fixed, permeabilized and immunostained as previously described.[11] The maintenance of the stem phenotype was determined by immunopositive Nestin labeling (1 : 200, ab6142, Abcam, United Kingdom). Cell commitment towards neuronal lineage was determined by positive staining for DCX (1 : 300, sc8066, Santa Cruz, USA) and MAP2 (1 : 500, ab5392, Abcam, United Kingdom). On the other hand, the commitments towards astroglial and oligodendroglial cell lineages were determined using GFAP (1 : 500, G9269, Sigma-Aldrich, USA), S100β (1 : 200, Dako Cytomation, Denmark) and Olig2 (1 : 200, MABN50, Millipore, USA). Alexa Fluor donkey anti-mouse, anti-rabbit, anti-goat or anti-chicken secondary antibodies coupled with 488 or 594 fluorophores (1 : 200, Life Technologies, USA) and goat anti-chicken Texas Red (1 : 200, ab6875, Abcam, United Kingdom) were used as secondary antibodies. To study the migration of cells into the hydrogels, serial cuts of 250 μm thickness slices of previously immunostained and 1% agarose embedded hydrogels were made and collected using a Microm HM650 V vibratome (Microm, International GmbH, Walldorf, Germany).

2.3.4. RNA extraction and quantitative retro transcriptase (RT) polymerase chain reaction (qPCR). After 7, 14 or 21 days in culture, NSCs were washed with PBS and the RNA extracted using the RNAqueous kit (AM1906/AM1931; Ambion Life technologies, Waltham, Massachusetts, USA). The isolated RNA purity was verified by the Nanodrop Synergy HT (BioTek Agilent, Santa Clara, California, USA). Afterwards, iScript cDNA kit was used to obtain the cDNA (50 ng L^{-1}) from the extracted RNA by reverse transcription. Primer pairs utilized were retrieved from the PrimerBank using the PrimerBlast method and are summarized in Table 1.

For the quantitative PCR, 4.5 μL of SsoAdvanced Universal SYBR® Green Supermix (1725271; BioRad, Hercules, California, USA) were mixed with 0.5 μL of primers (0.3125 M), 0.3 μL of cDNA (1.5 ng μL^{-1}) and the necessary nuclease free water to reach 10 μL final volume reaction per well. Each primer was evaluated for optimal efficacy (>90%) and single product amplification using the melting curve approach. The $2^{-\Delta\Delta Ct}$ technique was employed to determine the relative expression of each gene, with *Gapdh* serving as internal control.[11,21] qPCR was carried out in triplicate using an ABI PRISM® 7000 (Thermo Fisher Scientific, Waltham, Massachusetts, USA). Data were examined using the CFX Manager™ program. For statistical analysis, 3 independent hydrogels were analyzed, and each of the samples measured in triplicate.

2.3.5. Intracellular reactive oxygen species measurements. To study the antioxidant benefits of the CeO_2 nanoparticles, NSCs were seeded over GO : AsA 1 : 1; GO : AsA 1 : 4 and GO : AsA 1 : 4 + CeO_2 0.25 hydrogels. After 14 days *in vitro*, NSCs were labeled with 50 μM of the 2′,7′-dichlorodihydrofluorescein diacetate cell-permeable probe (H2DCFDA, Invitrogen, USA) for 30 min at 37 °C and 5% CO_2 to evaluate the accumulation of reactive oxygen species (ROS) within cells. Fluorescence intensity of 3 independent samples of each condition was determined on Fluoroskan Ascent plate fluorimeter (Thermo Labsystems, Santa Rosa, California, USA) to determine the fluorescence intensity (λ_{ex} = 488 nm/λ_{em} = 520 nm) in the area.

2.3.6. Cell count and statistical analysis. Cell counts for each condition were performed in triplicate samples taking five aleatory hydrogel images of 0.1 mm^2. The total number of cells was counted using nuclear DAPI staining and the percentage of positive cells was determined in double-blinded cell counts for each respective marker with respect to the total number of cells. The results were presented as the mean average ± SD or SEM. Multiple group comparisons were done with One-way ANOVA, non-parametric Holm–Šídák test. $*p < 0.05$ was considered as statistically significant.

3. Results and discussion

3.1. Effect of AsA on the morphology, mechanical and electrical conductivity of the self-assembled three-dimensional hydrogels

Graphene oxide (GO) is a carbon-based material bearing oxygenated functional groups, which improve the solubility and

Table 1 List of primers used

Primers	Sequence 5′–3′	Lenght	Annealing	Amplicon (bp)
Gapdh (upstream)	GTATGACTCCACTCACGGCAA	21	61.8	274
Gapdh (downstream)	CTTCCCATTCTCGGCCTTG	19	60.2	274
Nestin (upstream)	CCCTGAAGTCGAGGAGCTG	19	61.4	166
Nestin (downstream)	CTGCTGCACCTCTAAGCGA	19	61.7	166
Gfap (upstream)	CTGGACTGCGTCATTTTCCC	20	59.2	256
Gfap (downstream)	CGATGGAGCCTCAGGGATGA	20	61.1	256
S100β (upstream)	TGGCTGCGGAAGTTGAGATT	20	59.9	84
S100β (upstream)	ATGGCTCCCAGCAGCTAAAG	20	60.1	84
Olig2 (upstream)	GTGGATGCTTATTACAGACC	20	56.1	94
Olig2 (downstream)	ACCTTCCGAATGTGAATTAG	20	58.1	94
Map2 (upstream)	GAAGAAACAGCTAATCTGCC	20	58.1	423
Map2 (downstream)	CTCTTGCTTATTCCATCAGTG	21	59.0	423
Dcx (upstream)	TCAGCATCTCCACCCAACCA	20	61.1	94
Dcx (downstream)	TTGTGCTTTCCCGGTTGACA	20	60.3	94

induce the expansion of the interlayer distance in aqueous solutions.[22] The reduction of the GO provokes the deletion of oxygen and other atomic-scale lattice defects, thus enhancing the hydrophobic nature and promoting the accumulation of the sheets *via* non-covalent interactions (Fig. 1A).[22,23] GO can be reduced in several ways, including chemical, thermal, electrochemical or light-driven approaches.[22,24] Chemical reduction, in combination with thermal annealing, results more effective in repairing vacancy defects and removing out-of-plane carbonyl groups.[22] Herein, we combined the chemical reduction with an overnight thermal treatment at 60 °C, using AsA as a reducing agent to overcome the limitations of more toxic alternatives.[25] This represents an easy and quick manner to synthesize 3D hydrogels by self-assembly with high C/O ratios without compromising mechanical and electrical properties.[25,26]

The absence or presence of oxygen functionalities will therefore have a direct impact on the final properties of the hydrogels.[27] The different proportions of GO : AsA allowed us to modulate both the reduction level and the arrangement of the GO sheets, which determined the pore size of the hydrogels (Fig. 1B). Scanning electron micrographs revealed the large porous structures formed by atomic wide walls of GO sheets. Increasing the amount of AsA diminished the repulsion forces between the GO sheets and enabled the formation of more compact structures with smaller pores. The GO : AsA 1 : 1 hydrogel showed the largest pores (7.3 ± 0.6 μm) with respect to the other two formulations (*i.e.*, GO : AsA 1 : 4 showing pores of 3.9 ± 0.2 μm & 1 : 10 with pores of 4.3 ± 0.5 μm). In agreement with these results, X-ray diffraction demonstrated that the addition of an increasing amount of AsA triggered the reduction of GO sheets, resulting in the dis-

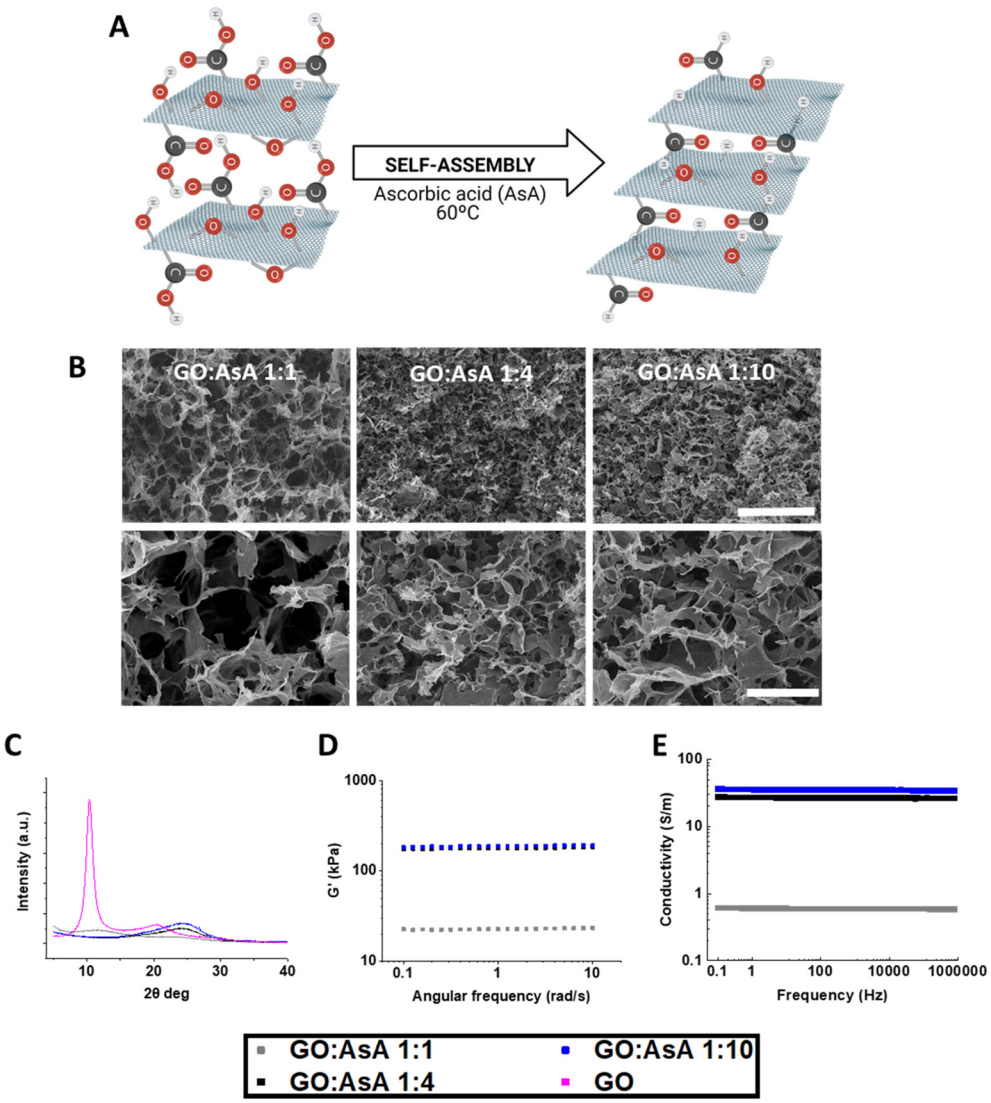

Fig. 1 Physicochemical characterization of GO : AsA hydrogels. (A) Schematic representation of the reduction process and self-assembly of the hydrogels. (B) SEM images of the GO : AsA 1 : 1, GO : AsA 1 : 4 and GO : AsA 1 : 10 hydrogels. Scale bar 100 μm on the upper images and 20 μm on the lower images. (C) XRD spectra, (D) shear modulus determined by rheology and (E) electrical conductivity of the hydrogels.

placement of the diffraction peak to higher values (*i.e.*, from 10° in the commercial GO to 24° in the GO : AsA 1 : 4 & 1 : 10) (Fig. 1C). According to Bragg's law, the interlayer distance of the commercial GO was 0.85 nm and decreased till 0.77 nm in the GO : AsA 1 : 1 sample. The chemical reduction of GO stimulated the self-assembly of the reduced GO sheets thanks to the reduction of hydroxyl, epoxy, carboxyl and carbonyl groups,[28] that enabled the formation of new π–π binding sites between the GO sheets. The deletion of oxygenated functional groups also raised the hydrophobicity of the graphene sheets. The combined effect of these two events provoked a random overlapping of flexible graphene sheets, thus favouring the self-assembly of the 3D hydrogels. Remarkably, the addition of more AsA decreased the interlayer distance in the GO : AsA 1 : 4 and GO : AsA 1 : 10 hydrogels till 0.37 nm in both cases, but no differences were observed between these two formulations, suggesting that the reduction level was similar in both cases. These results were further corroborated by XPS (ESI Fig. 1†). The addition of AsA at a GO : AsA 1 : 1 ratio clearly reduced the area associated to oxygen functionalities with respect to the original GO. Oxygen functionalities were further reduced in the GO : AsA 1 : 4 ratio but no significant differences were observed when the GO : AsA ratio was increased to 1 : 10, suggesting that the maximum level of reduction had been reached. As observed, the reduced graphene oxide hydrogels still contain oxygen functionalities in their structure, which are absent in the structure of pure graphite.

The mechanical properties of the hydrogels were measured by rheology. The GO : AsA 1 : 1 hydrogel showed the lowest shear modulus (G') (22.8 ± 0.3 kPa), which in viscous materials is directly correlated with the elastic capabilities (Fig. 1D). The GO : AsA 1 : 4 and GO : AsA 1 : 10 presented increased shear modulus (178.4 ± 2.8 kPa *vs.* 186.4 ± 2.6 kPa), demonstrating the modulation of the mechanical properties in almost one order of magnitude by controlling the reduction level through simply modifying the amount of AsA added. As shown in other studies and by us, once the maximum reduction level is achieved, the mechanical properties of the hydrogels remain stable.[29] Although the human brain presents a low shear modulus of around 1–2.5 kPa,[30] other central nervous system areas like the spinal cord recorded shear modulus of 250–300 kPa[31] and the peripheral nervous system like ulnar and median nerves register a shear modulus around 10–20 kPa,[32] which are similar to the mechanical properties presented by our hydrogels. Besides, it is reported the acquirement of well differentiated neural cultures of stem cells *in vitro* and *in vivo* with scaffolds that present even higher stiffness values,[33] suggesting that all the hydrogels exhibited mechanical properties compatible with neural differentiation of stem cells.

GO is a poor electrical conductor due to the lack of percolating conduits between sp^2 carbon atoms that act as electron carriers in graphene. The reduction process with AsA induces the deletion of oxygen functionalities and raises the amount of sp^2 or π–π binding sites which consequently increases the conductivity of the material.[34] In accordance with the data of other studies,[35] the electrical conductivity of the hydrogels increased with the addition of AsA. The GO : AsA 1 : 1 hydrogel exhibited the lowest electrical conductivity (0.6 S m^{-1}), which increased in GO : AsA 1 : 4 (27 S m^{-1}) and GO : AsA 1 : 10 (35 S m^{-1}) (Fig. 1E). Accordingly, we were able to enhance the electrical conductivity thanks to the deletion of atomic-scale lattice defects of the GO sheets *via* the thermochemical reduction process.[22] According to these results, other groups have reported electrical conductivities between 0.045 and 600 S m^{-1} on graphene-based hydrogels.[36–38] Remarkably, as it has been previously reported, the impedance or the electrical conductivity are constant in graphene oxide as usually observed for highly conducting systems.[39,40] The human brain has an electrical conductivity of around 0.33 S m^{-1}, where grey matter exhibits a conductivity of around 0.47 ± 0.24 S m^{-1} and white matter around 0.22 ± 0.17 S m^{-1}.[41,42] However, materials showing electrical conductivity values between 0.08–1.3 S m^{-1} or even higher values are able to electrically stimulate neurons.[43,44] Therefore, all our hydrogels showed conductivity values compatible with neural stimulation.

3.2. Effect of CeO_2 nanoparticles on the morphology, mechanical, electrical and antioxidant properties of the self-assembled three-dimensional hydrogels

Cerium oxide (CeO_2) nanoparticles are widely known for possessing antioxidant and neuroprotective properties.[45] Here, CeO_2 nanoparticles were incorporated during the self-assembly of the graphene-based hydrogels, a process that is favored by electrostatic interactions between the negatively charged GO sheets (−29.1 ± 0.36 mV) and the positively charged CeO_2 nanoparticles (24.3 ± 0.57 mV), as demonstrated by dynamic light scattering (DLS) (Fig. 2A and B).

To confirm the presence of CeO_2 nanoparticles in our samples, we performed transmission electron microscopy (TEM). TEM micrographs showed the GO sheets successfully decorated with CeO_2 nanoparticles prior to their reduction with AsA (Fig. 2C). Moreover, the amount of CeO_2 nanoparticles on the surface of the GO sheets increased with the addition of more CeO_2 to the samples (data not shown). These results were further corroborated with Raman spectroscopy and energy-dispersive X-ray spectrometry (EDX) (Fig. 2D, E and ESI Fig. 2†). Raman spectroscopy demonstrated that all the samples that contained CeO_2 nanoparticles showed a band at 453 cm^{-1} that can be ascribed to the first order scattering of CeO_2[46] and increased in intensity as the amount of CeO_2 nanoparticles raised. As expected, the GO : AsA 1 : 4 sample only exhibited the characteristic D and G bands (1350 and 1580 cm^1 respectively) which are related to the disarranged sp^2-hybridized carbon structure and expansion of the C–C bond in graphitic materials.[11,47] In accordance with these results, EDX demonstrated the presence of Ce in the samples containing CeO_2 nanoparticles and presented similar proportions for carbon (C) (73.22–79.74%) and oxygen (O) (19.75–25.19%) in all the samples.

SEM images demonstrated that, despite the addition of CeO_2 nanoparticles, hydrogels preserved their highly porous structures formed by atomic wide walls of GO sheets (Fig. 2F).

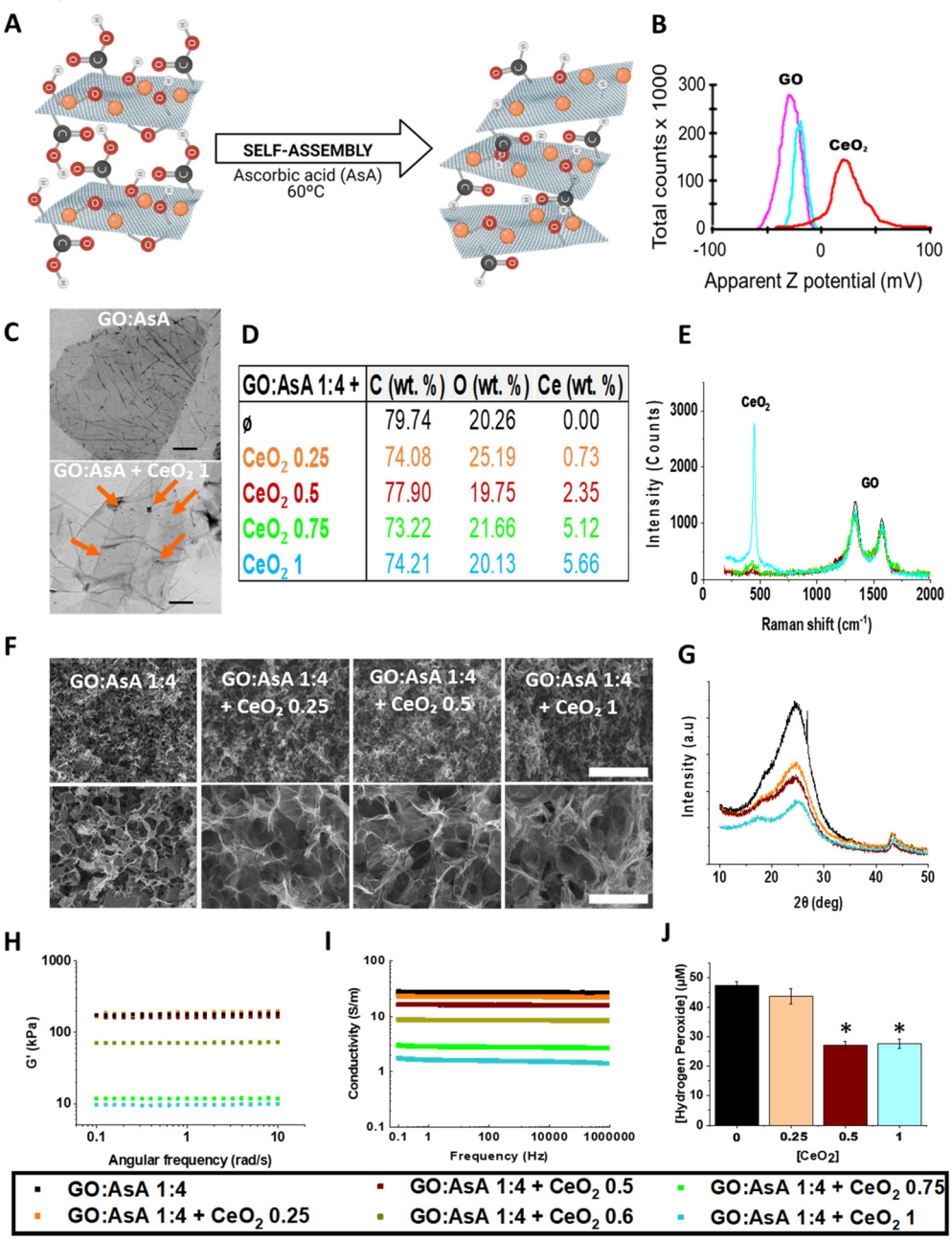

Fig. 2 Physicochemical characterization of GO : AsA + CeO_2 nanoparticles hydrogels. (A) Schematic representation of the decoration of the GO sheets with CeO_2 nanoparticles (orange) and the subsequent self-assembly process. (B) Dynamic light scattering (DLS) measurements showing the negatively charged GO sheets in pink, the positively charged CeO_2 nanoparticles in red and the shift on the electronegativity of the GO sheets when combined at a GO : CeO_2 10 : 1 proportion in light blue. (C) TEM micrographs showing the GO sheets decorated with CeO_2 nanoparticles. Orange arrows highlight the presence of CeO_2 nanoparticles. Scale bar 1 μm on top and 200 nm in the bottom image. (D) EDX analysis showing the C, O and Ce wt%. (E) Raman spectra and (F) SEM images of the GO : AsA 1 : 4, GO : AsA 1 : 4 + CeO_2 0.25, GO : AsA 1 : 4 + CeO_2 0.5 and GO : AsA 1 : 4 + CeO_2 1 hydrogels. Scale bar 100 μm on the upper images and 20 μm on the lower images. (G) XRD spectra of the hydrogels with different amounts of CeO_2 nanoparticles. (H) Shear modulus determined by rheology, (I) electrical conductivity and (J) antioxidant capacity of the hydrogels. *$p < 0.05$ compared to GO : AsA 1 : 4, Holm–Šídák method One Way Analysis of Variance on Ranks.

The estimated pore size was, however, slightly reduced after the incorporation of CeO_2 nanoparticles. Accordingly, the estimated pore size were 3.9 ± 0.2 μm, 2.1 ± 0.1 μm, 2.6 ± 0.2 μm and 2.7 ± 0.2 μm for GO : AsA 1 : 4, GO : AsA 1 : 4 + CeO_2 0.25, GO : AsA 1 : 4 + CeO_2 0.5 and GO : AsA 1 : 4 + CeO_2 1, respectively. The XRD showed a peak at 24° in all the samples (Fig. 2G), demonstrating that the interlayer distance was not affected by the addition of CeO_2 nanoparticles. Nevertheless, the intensity of the peak dropped down with the addition of CeO_2 nanoparticles to the samples in a dose dependent

manner, denoting an interlayer distortion of the GO sheets, mediated by the CeO_2 nanoparticles. Remarkably, in all the samples there was a peak at 43° which corresponded to the plane of the graphene layer[48] and indicated that the CeO_2 nanoparticles were localized on the interlayer space without inducing any variation in the GO sheets.[49]

The mechanical behavior of the hydrogels decorated with CeO_2 nanoparticles was again measured by rheology. The GO : AsA 1 : 4 + CeO_2 0.25 and GO : AsA 1 : 4 + CeO_2 0.5 (187.7 ± 7.5 kPa and 164.6 ± 1.6, respectively) showed a shear modulus similar to the GO : AsA 1 : 4 hydrogel (178.4 ± 2.8 kPa). A gradual decrease on the mechanical properties was however observed in the GO : AsA 1 : 4 + CeO_2 0.6 (71.6 ± 0.7 kPa), GO : AsA 1 : 4 + CeO_2 0.75 (11.8 ± 0.1 kPa) and GO : AsA 1 : 4 + CeO_2 1 (9.7 ± 0.1 kPa) hydrogels (Fig. 2H). The fact that the shear modulus decreased with the addition of more CeO_2 nanoparticles to the samples indicated the possibility to tune the mechanical properties of the hydrogel by just modifying the CeO_2 nanoparticle concentration. These results are in line with those obtained by other groups using dopant nanoparticle substances like platinum[50] and can be explained due to the less organized structures associated to the incorporation of the CeO_2 nanoparticles in the interlayer space of the GO sheets, as suggested by XRD.

We also measured the electrical properties of the hydrogels. GO : AsA 1 : 4 + CeO_2 0.25 and GO : AsA 1 : 4 + CeO_2 0.5 (22 S m^{-1} and 17 S m^{-1}) maintained almost the same electrical conductivity of the GO : AsA 1 : 4 (27 S m^{-1}) (Fig. 2I). However, the addition of an increasing amount of CeO_2 nanoparticles resulted in a decline of the electrical conductivity of the GO : AsA 1 : 4 + CeO_2 0.6, GO : AsA 1 : 4 + CeO_2 0.75 and GO : AsA 1 : 4 + CeO_2 1 hydrogels (8.5 S m^{-1}; 2.8 S m^{-1} and 1.6 S m^{-1} respectively), which may be attributed to the more disordered arrangement of the GO sheets due to the incorporation of the CeO_2 nanoparticles in the interlayer space. Nevertheless, the electrical values obtained proved that all our hydrogels could potentially trigger the electrical excitation of the seeded neural cells.[43,44]

It is well known that cerium oxide can exhibit +3 and +4 states that support the formation of CeO_2 and CeO_{2-x} and provides antioxidant properties.[51] CeO_2 nanoparticles resemble the antioxidant enzymes superoxide dismutase (SOD) and catalase (CAT) and, hence, scavenge reactive oxygen species (ROS) and free radicals[51,52] in physiological conditions.[45,53,54] Here, we applied a concentration of 50 μM hydrogen peroxide (H_2O_2) and measured the antioxidant capabilities of the hydrogels containing increasing amounts of CeO_2 nanoparticles. It was reported in the literature that this H_2O_2 concentration is able to mimic the pro-oxidative environment found *in vivo* which may cause a detrimental effect on important cellular structures, thus leading to oxidative distress.[55] As expected, all the hydrogels containing CeO_2 nanoparticles were able to reduce the hydrogen peroxide concentration in a dose dependent manner. In contrast, the GO : AsA 1 : 4 sample had no antioxidant properties, demonstrating that the CeO_2 nanoparticles were responsible of the decline on the hydrogen peroxide concentration (Fig. 2J). These results are in agreement with other studies were CeO_2 nanoparticles have demonstrated to possess antioxidant properties *in vitro* and *in vivo*, creating a more favorable microenvironment for angiogenesis and nerve reconstruction, resulting accordingly in a neuroprotective effect.[18,56]

3.3. Adhesion and integration of NSCs on the hydrogels

Materials based on graphene derivatives, when arrested in hydrogel form, have been shown not only to minimize the direct toxicity on cells, but also to promote the growth and differentiation of neural cells.[57] Herein, we explored the effect of different configurations of GO-based hydrogels with varying morphological, mechanical and electrical properties (which are dependent on one another) on the neural commitment of NSCs. Thus, the GO : AsA 1 : 1 hydrogel, which exhibited the largest pores and lowest stiffness and electrical conductivity, was compared with the GO : AsA 1 : 4, which exhibited smaller pores, but higher stiffness and electrical conductivity. To compare the influence of the CeO_2 nanoparticles on the neural differentiation, the GO : AsA 1 : 4 + CeO_2 0.25 hydrogel was selected, which exhibited morphological, electrical and mechanical properties comparable to the GO : AsA 1 : 4 one.

NSCs were seeded directly on the hydrogels and, as shown by SEM micrographs, were able to attach without a need of Fetal Bovine Serum (FBS) supplementation or extracellular matrix (ECM)-derived compound coating in 24 h (ESI Fig. 3†). They could even migrate inside the hydrogels after 7 days in culture (ESI Fig. 4†), demonstrating a good infiltration of the cells in the material. Indeed, NSC survival, adhesion and infiltration are crucial to facilitate the bench to clinic implementation of these hydrogels. Besides, the use of ECM-derived coatings like laminin have been correlated with cell proliferation of brain cancers such ependymoma or glioblastoma.[58] Thus, by eluding its use, we also avoid the possibility of having degradation products that could represent a lethal risk in clinical approaches.[59] In the same way, fetal serum supplementation in cell culture has been ascribed to be strongly immunogenic in both rodents and humans. Hence, by eluding its use in here, we also maximize the bench to clinic translation potential of our systems.

To assess the impact of the hydrogels on the establishment of a heterogeneous culture for future neural regeneration, after 7, 14 and 21 days *in vitro* (DIV), cells were fixed and immunostained for neural stem (Nestin), astroglial (GFAP and S100β), oligodendroglial (Olig2) or neuronal lineage markers (DCX and MAP2) to study the effect of each hydrogel on the differentiation fate of the NSCs. Additionally, RNA was extracted and quantitative retro transcriptase polymerase chain reaction (qPCR) was performed against Nestin, GFAP, S100β and MAP2 to better characterize the gene expression profile at messenger RNA (mRNA) level and corroborate the immunolabeling results.

3.4. Stemness and glial cell differentiation of NSCs on the hydrogels

The maintenance of the NSC phenotype of the seeded cells was assessed by the presence of the intermediate filament

Nestin. Nestin is a marker of neural precursor cells in embryonic and adult CNS tissue[60] and it is also considered to be a multipotent stem cell marker with crucial regulatory roles on the proliferation of immature cells[61] including neural progenitor cells.[62,63] Thus, non-differentiated NSCs are characterized by the expression of both Nestin and GFAP markers, but during the differentiation process, Nestin is progressively downregulated and replaced by other markers of more differentiated cells.[64] We found that GO : AsA 1 : 4 + CeO_2 0.25 hydrogel showed a more rapid decrease in the proportion of the Nestin positive stem cell population, suggesting a faster differentiation of the seeded NSCs to mature neuronal and glial cell lineages (3.7 ± 0.2%, $p < 0.05$), followed by the GO : AsA 1 : 4 (28.4 ± 2.2%, $p < 0.05$) and the GO : AsA 1 : 1 (37.8 ± 6.4%, $p < 0.05$) at DIV7 (Fig. 3B). To further corroborate our findings, the messenger mRNA was analysed by qPCR. GO : AsA 1 : 4 + CeO_2 0.25 exhibited very little Nestin expression at DIV7 (0.03 ± 0.01, fold change, $p < 0.05$) with respect to the control GO : AsA 1 : 1 hydrogel (Fig. 3C). By DIV21, Nestin expression was progressively lost in all the conditions, showing the exhaustion and eventual replacement of the stem cell population with mature differentiated neuronal and glial cells, in the presence of differentiation inducing media. Interestingly, in GO : AsA 1 : 4 + CeO_2 0.25 hydrogels the proportion of Nestin positive cells still showed a significant peak at DIV14 (34.0 ± 6.7%, $p < 0.05$) compared to the other two conditions (GO : AsA 1 : 1 10.6 ± 2.2% and GO : AsA 1 : 4 0.6 ± 0.1%, $p < 0.05$) which had almost completely depleted the non-differentiated NSC population by that time (Fig. 3B). This suggested that between DIV7 and DIV14 the NSCs seeded on the GO : AsA 1 : 4 + CeO_2 0.25 hydrogel still underwent several rounds of cell division, contrary to the other two hydrogels. This result seems to be related to a higher antioxidant capacity, which is associated with a better survival and maintenance of self-renewal in many types of stem cells, including NSCs.[65] At mRNA level, Nestin expression was also clearly increased at DIV14 in the GO : AsA 1 : 4 + CeO_2 0.25 hydrogels, in comparison to GO : AsA 1 : 1 and GO : AsA 1 : 4 (Fig. 3C). Thus, the NSC population was preserved for longer times up to DIV14 in the GO : AsA 1 : 4 + CeO_2 0.25 hydrogel, a fact which could be attributed to its antioxidant properties.[65] It is well known that inflammation and oxidative stress, which are intimately linked to each other,[66] are detrimental to NSC activation and neurogenesis.[67] Therefore, the improved antioxidant capacity of the GO : AsA 1 : 4 + CeO_2 0.25 hydrogel would also contribute to a maintenance of non-differentiated NSCs on the medium term (DIV14), despite their enhanced response to the initial wave of cell differentiation triggered by the soluble factors of the culture medium at DIV7. Non-differentiated NSCs can secrete neurotrophic factors that protect the developing neural tissue and help on its regeneration process.[68] Therefore, the better preservation of stem cells on the GO : AsA 1 : 4 + CeO_2 0.25 hydrogel might be helpful for the generation of a functional neural tissue *in vitro*.

NSC are remnant cells of the CNS development restricted in neurogenic niches and maintain the ability to differentiate towards neuronal and glial lineages.[69] A balanced neuronal and glial cell differentiation is important for the long-term survival of the NSC-derived cell cultures due to the supporting function of the glial cells over the new-born neurons on the regulation of their oxidative and metabolic balance, and the neurophysiological processes of ion and neurotransmitter uptake and release, among others.[11,70]

We also characterized the NSC differentiation process towards astroglial lineages, by the loss of Nestin, the increase of the expression of glial fibrillary acidic protein (GFAP) and the appearance of the S100 calcium-binding protein β (S100β) marker during the astroglial differentiation (Fig. 3 and 4). The percentage of GFAP positive cells at DIV7 indicated that GO : AsA 1 : 4 substrate promoted more astroglial differentiation (22.6 ± 8.2%, $p < 0.05$) than GO : AsA 1 : 1 (5.6 ± 3.4%, $p < 0.05$) or GO : AsA 1 : 4 + CeO_2 0.25 (3.7 ± 0.2%, $p < 0.05$) hydrogels (Fig. 3B). At mRNA level, GO : AsA 1 : 4 also exhibited a higher expression of GFAP (9.7 ± 1.7, fold change, $p < 0.05$), in comparison with GO : AsA 1 : 1 (1.0 ± 0.2, fold change, $p < 0.05$) and GO : AsA 1 : 4 + CeO_2 0.25 (0.7 ± 0.1, fold change, $p < 0.05$) (Fig. 3C). These results suggested that, as previously described, stiffer substrates like GO : AsA 1 : 4 promoted the differentiation towards glial lineages compared to softer ones.[71,72]

However, the presence of CeO_2 nanoparticles could modulate the final fate of this astroglial phenotype into not only astrocytes, but also other types of glial cells or even the enhanced maintenance of non-differentiated stem cell phenotypes. In this sense, GO : AsA 1 : 4 + CeO_2 0.25 exhibited an augmented GFAP expression on mRNA level at DIV14 (66.3 ± 2.4, fold change, $p < 0.05$), in comparison with GO : AsA 1 : 1 (9.3 ± 2.8, fold change, $p < 0.05$) and GO : AsA 1 : 4 (12.7 ± 2.6, fold change, $p < 0.05$) (Fig. 3C). However, this expression was correlated with a similar increase on Nestin mRNA level, suggesting a possible expansion of the NSC population, rather than an astroglial cell differentiation. Indeed, the co-expression of GFAP and Nestin has been ascribed to the stem phenotype of neural cells and their proliferation.[73,74]

Interestingly, at DIV21 we found an abundant GFAP positive astroglial cell subpopulation with no Nestin expression in GO : AsA 1 : 1 (36.5 ± 1.8%, $p < 0.05$) and GO : AsA 1 : 4 (31.1 ± 1.7%, $p < 0.05$) hydrogels, compared to GO : AsA 1 : 4 + CeO_2 0.25 hydrogels where those GFAP + cells were relatively much less frequent (1.7 ± 0.1%, $p < 0.05$) (Fig. 3B). At mRNA level, GO : AsA 1 : 1 also exhibited a higher GFAP expression with respect to DIV7 (20.8 ± 0.9, fold change, $p < 0.05$), almost equaling the levels of the GO : AsA 1 : 4 (25.5 ± 0.8, fold change, $p < 0.05$). Remarkably, GO : AsA 1 : 4 + CeO_2 0.25 exhibited a lower GFAP mRNA expression (11.2 ± 2.2, fold change, $p < 0.05$) further corroborating the finding of the immunofluorescence assays (Fig. 3C).

From the perspective of tissue engineering therapies, the presence of GFAP positive astrocytes may pose both advantages and disadvantages. On the one hand, mature astrocytes are an important supporting glial cell of the CNS, sustaining neuronal metabolism and function. On the other hand, astroglial

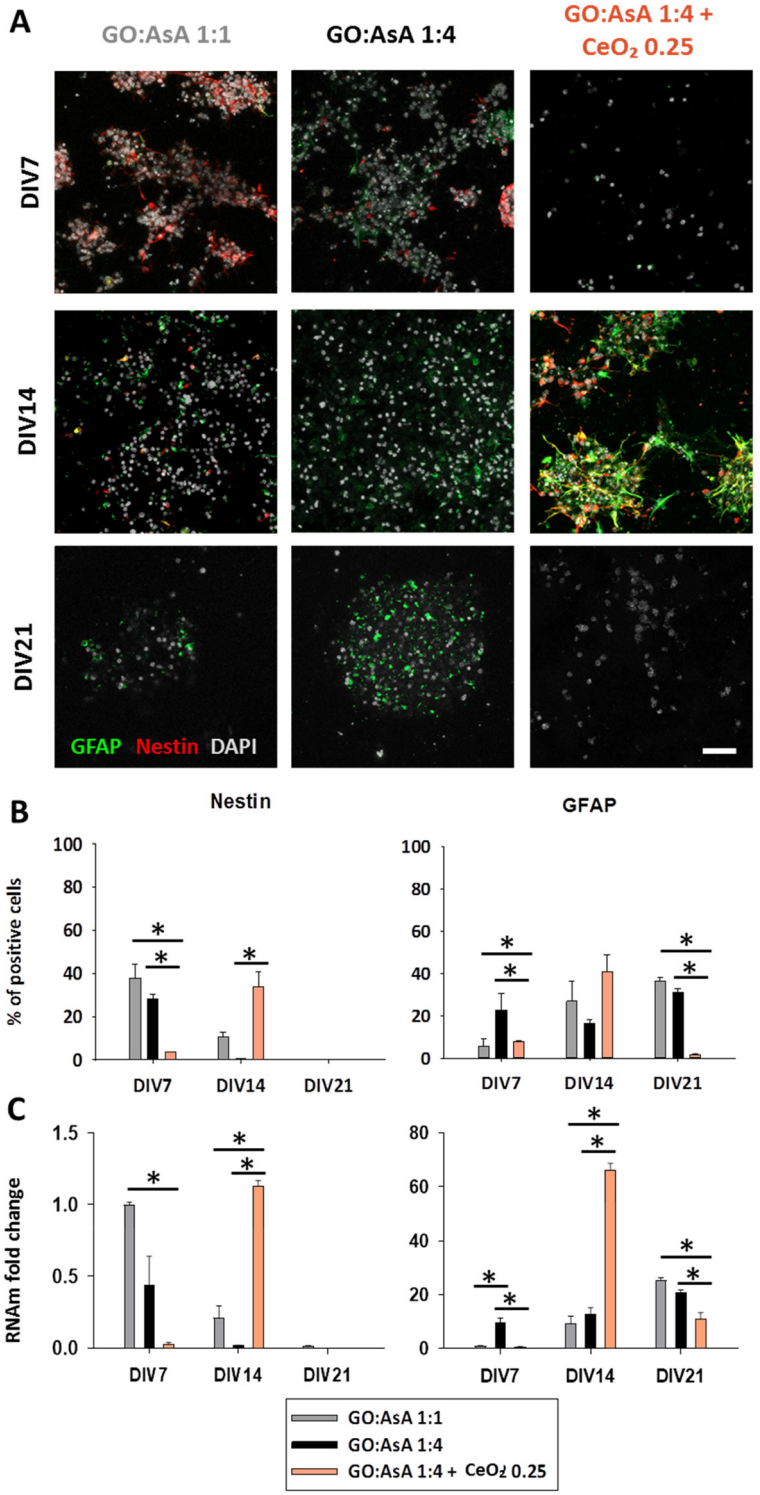

Fig. 3 Immunofluorescence showing immature neural stem phenotype cells on the hydrogels. (A) Double immunofluorescence showing GFAP (green) positive cells together with Nestin (red) stem-like cells positive cells in GO : AsA 1 : 1, GO : AsA 1 : 4 and GO : AsA 1 : 4 + CeO_2 0.25 hydrogels after DIV 7, 14 and 21. Scale bar 50 μm. (B) Quantification of the percentage of positive cells of each of the markers tested (C) qPCR measurements showing the fold change compared to GO : AsA 1 : 1 hydrogel at DIV7. (*p < 0.05 compared to the other hydrogels at the same time-points. Holm–Šídák method One-way ANOVA Analysis of Variance on Ranks).

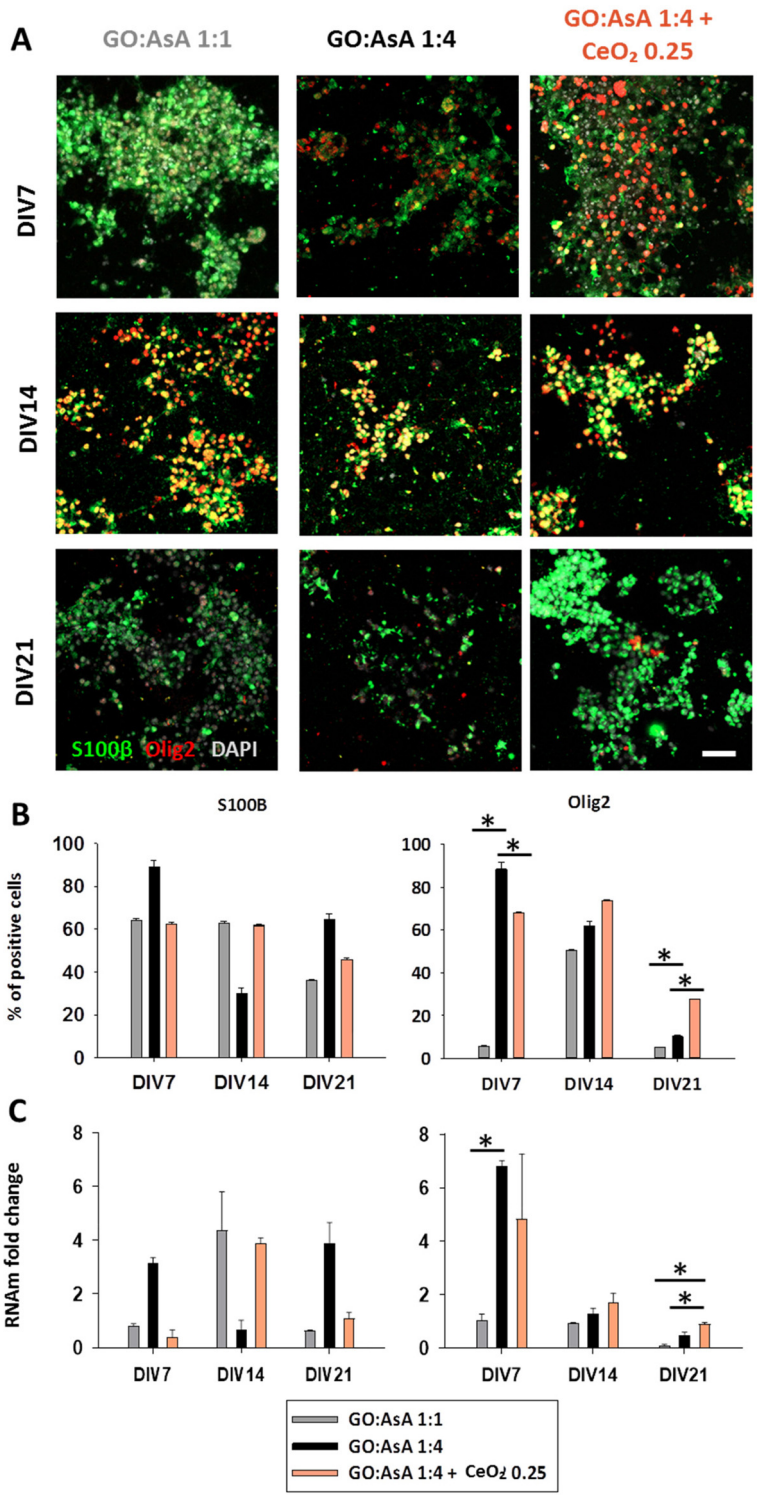

Fig. 4 Immunofluorescence showing astroglial and oligodendroglial differentiation on the hydrogels. (A) Double immunofluorescence showing S100β (green) mature astroglial and Olig2 (red) positive oligodendroglial-like cells in GO : AsA 1 : 1, GO : AsA 1 : 4 and GO : AsA 1 : 4 + CeO_2 0.25 hydrogels after DIV 7, 14 and 21. Scale bar 50 μm. (B) Quantification of the percentage of positive cells of each of the markers tested (C) qPCR measurements showing the fold change compared to GO : AsA 1 : 1 hydrogel at DIV7. (*$p < 0.05$ compared to the other hydrogels at the same time-points. Holm–Šídák method One-way ANOVA Analysis of Variance on Ranks).

cells have also been described to be involved in glial scar formation after CNS injury.[75] Scar tissue has a dual component: first, the glial scar formed by glial precursors, reactive astrocytes and microglia found at the periphery of the lesion, and second, the fibrotic scar composed by phagocytic cells and fibroblasts at the lesion core.[76] This biological process has been reported detrimental for an effective reinnervation of the damaged CNS.[77] Taking into account that reactive astroglial phenotypes can be induced when these cells are exposed to a damaged CNS environment, the presence of high amounts of astrocytes (GFAP positive astroglial subpopulation) in the tissue engineered grafts may constitute a limitation for therapeutic purposes.[76]

During the maturation of the astrocytes, together with the expression of GFAP, cells acquire the expression of S100β.[78,79] All the tested hydrogels presented a mature astroglial-like lineage population over time since the proportion of S100β positive cells were always higher than that of GFAP positive cells in all the conditions at protein level (Fig. 4A and B). qPCR results further corroborated the presence of S100β protein in all the conditions and demonstrated a higher expression of S100β mRNA on GO : AsA 1 : 4 (3.9 ± 0.8 fold change, $p < 0.05$) at DIV21, compared to GO : AsA 1 : 1 (0.6 ± 0.0 fold change, $p < 0.05$) and GO : AsA 1 : 4 + CeO_2 0.25 (1.1 ± 0.2 fold change, $p < 0.05$) (Fig. 4C), suggesting a possible establishment of a mature astroglial differentiation on the stiffer hydrogels with smaller pores and greater mechanical and electrical properties. It is noteworthy that S100β, apart from mature astroglial cells, is also a marker of oligodendroglial lineage cells.[80] Oligodendrocyte precursors are known to express both S100β and Olig2 markers.[80] Therefore, in view of this result, we also studied the expression of oligodendrocyte transcription factor Olig2 on the cell-seeded hydrogels. The expression of Olig2 in oligodendrocyte progenitors has been reported to be increased during the remyelination process of injured axons in multiple sclerosis (MS),[81] and is characteristic of an *in situ* expanding oligodendrocyte population. At DIV7, the proportion of the oligodendroglial lineage population on the GO : AsA 1 : 1 (5.9 ± 0.4%, $p < 0.05$) was also lower compared to GO : AsA 1 : 4 (88.5 ± 3.0%, $p < 0.05$) and GO : AsA 1 : 4 + CeO_2 0.25 (68.2 ± 0.2%, $p < 0.05$) (Fig. 4B). These results were further corroborated at mRNA level, where GO : AsA 1 : 4 at DIV7 exhibited a significantly higher Olig2 expression (6.8 ± 0.2, fold change, $p < 0.05$) compared to GO : AsA 1 : 1, demonstrating again that stiffer substrates promoted a faster differentiation towards glial cell lineages (Fig. 4C).

Interestingly, GO : AsA 1 : 4 + CeO_2 was able to support much better the oligodendroglial cell population for long culture periods until DIV21 (27.6 ± 0.2%, $p < 0.05$) compared to GO : AsA 1 : 1 (5.4 ± 0.1%, $p < 0.05$) and GO : AsA 1 : 4 (10.3 ± 0.5%, $p < 0.05$) (Fig. 4B), although at mRNA level all the hydrogels presented a decay on Olig2 expression (Fig. 4C). These results suggested that the presence of CeO_2 nanoparticles might have helped on the establishment of a mature and healthy oligodendroglial lineage subpopulation expressing Olig2 protein within the hydrogel. Oligodendrocytes are known to be a particularly sensitive cell type to oxidative stress.[82,83] Although the antioxidant effect of CeO_2 0.25 using a concentrated source of exogenous H_2O_2 was limited, it might modulate the physiological levels of intracellular free radicals, which may explain the beneficial effect of the CeO_2 nanoparticles addition on oligodendroglial survival in the scaffolds. Indeed, CeO_2 nanoparticles have been reported to possess antioxidant and neuroprotective capabilities and even attenuate the inflammation and help on the recovery of demyelinating pathologies like MS,[84] further suggesting their implication on oligodendrocyte function and survival. Our results also show that, even if no statistical difference was observed for the GO : AsA 1 : 4 + 0.25 CeO_2 formulation on H_2O_2 reduction, the added CeO_2 nanoparticles managed to decrease the accumulation of intracellular reactive oxygen species in NSCs (GO : AsA 1 : 1 100.0 ± 5.8, GO : AsA 1 : 4 88.7 ± 6.0 and GO : AsA 1 : 4 + CeO_2 0.25 48.7 ± 2.2, $p < 0.05$) (ESI Fig. 5†), enhancing the survival and modulating the differentiation pattern of these cells. This may be ascribed to the reduction of other reactive oxygen species or *via* other mechanisms beyond the scope of this study.

Overall, our results indicated that stiffer substrates like GO : AsA 1 : 4 promoted astroglial and oligodendrogial differentiation. Nevertheless, both GO : AsA 1 : 1 and GO : AsA 1 : 4 hydrogels were able to support a GFAP positive astrocyte-like subpopulation. Remarkably, the addition of CeO_2 nanoparticles on the GO : AsA 1 : 4 + CeO_2 hydrogel induced a much better maintenance of both Nestin + stem cell populations and also Olig2 + oligodendroglial lineage cell populations for longer culture periods until DIV21.

3.5. Neuronal differentiation pattern and establishment of neuron-oligodendrocyte co-cultures on graphene-derivatives and CeO_2 nanoparticles-based hydrogels

Glial cells play a key role on regeneration, but mature and immature neurons are also needed to promote and coordinate innervation and, hence, the regeneration process.[85] The presence of neuronal progenitor cells also needs to be assessed to predict an effective neuroregeneration outcome. Hence, we performed immunofluorescence labeling to detect the immature neuronal marker doublecortin (DCX).[86] DCX expression is restricted to neuronal lineage immature cells and multipotent-precursors in both the developing and adult brain[87] and also in regions of adult neurons undergoing a plastic reorganization of their dendrites.[88] We found that the GO : AsA 1 : 4 hydrogel was unable to support DCX positive cells at any of the periods tested and GO : AsA 1 : 1 only supported them until DIV7 (ESI Fig. 6†). By contrast, GO : AsA 1 : 4 + CeO_2 0.25 was able to maintain a substantial population of DCX positive cells until DIV21 (28.4 ± 0.3%, $p < 0.05$) (ESI Fig. 6B†). The qPCR further corroborated these findings, where GO : AsA 1 : 4 + CeO_2 0.25 (4.4 ± 0.9, $p < 0.05$) exhibited 4 times more DCX mRNA at DIV14 than GO : AsA 1 : 1 (0.7 ± 0.1) and GO : AsA 1 : 4 (0.2 ± 0.0) and 38 times more at DIV21 (GO : AsA 1 : 4 + CeO_2 0.25 (38.3 ± 10.3, $p < 0.05$) (ESI Fig. 6C†). These results may indicate the presence of DCX + multipotent-precursors and are

in accordance with the increase in Nestin positive cells that occurred in GO : AsA 1 : 4 + CeO_2 0.25 at DIV14. The persistence of DCX positive population in the GO : AsA 1 : 4 + CeO_2 0.25 hydrogels at DIV21 may be attributed to a better oxidative balance and long-term survival of neuronal lineage cells in culture, which are another very sensitive cell type to oxidative stress.[82]

The functionality and successful engraftment of bioengineered nerve tissues implies a balanced generation of both mature and immature glial and neuronal cells. Hence, we also studied the expression of other mature neuronal markers like microtubule-associated protein 2 (MAP2), which is expressed in the dendrites of fully mature neurons.[89] The percentage of MAP2 positive neurons in our hydrogels was much higher in GO : AsA 1 : 4 + CeO_2 0.25 (35.4 ± 0.2%, $p < 0.05$), than in GO : AsA 1 : 1 (0.04 ± 0.03% $p < 0.05$) and GO : AsA 1 : 4 (0.03 ± 0.02%, $p < 0.05$), which exhibited almost no mature neuronal generation at DIV7 (Fig. 5A and B). These results were further corroborated by qPCR, where GO : AsA 1 : 4 + CeO_2 0.25 exhibited a higher expression for MAP2 (26.1 ± 7.5 fold change, $p < 0.05$) compared to GO : AsA 1 : 1 and GO : AsA 1 : 4 at DIV7 (Fig. 5C). On the contrary, no MAP2 positive cells were ever found at any time point on GO : AsA 1 : 4 hydrogel, but qPCR results showed an increase on MAP2 expression at DIV21 (2.3 ± 0.7 fold change $p < 0.05$ compared to DIV7), suggesting a possible delay of the neuronal differentiation on stiffer substrates with smaller pores and greater electrical conductivity due to the favored differentiation towards astroglial lineages.[71,72] These results also corroborated the positive effect of the addition of CeO_2 nanoparticles for a quicker neuronal differentiation over GO based 3D materials.

Interestingly, GO : AsA 1 : 1 showed an increase on MAP2 positive cells (22.9 ± 0.4%, $p < 0.05$) at DIV14, and at DIV21 on mRNA content (9.4 ± 0.8 fold change, $p < 0.05$ compared to DIV7) (Fig. 5B and C). These results are in agreement with DCX results in GO : AsA 1 : 1 at DIV7, which exhibited an increase in DCX positive cells. It might be assumed that some of these progenitor cells would proceed through their differentiation process to eventually give rise to mature neurons at DIV14 and the higher expression of MAP2 at DIV21 and corroborates the findings of other studies in the literature, where softer substrates were reported to promote the differentiation towards neuronal lineages.[71,72]

However, the GO : AsA 1 : 1 hydrogel was unable to support the survival of the MAP2 positive cells for longer periods (Fig. 5B). On the contrary, the GO : AsA 1 : 4 + CeO_2 0.25 hydrogel managed to support a subpopulation of MAP2 positive mature neurons until DIV21. Our findings suggested that the addition of CeO_2 nanoparticles to the hydrogels allowed them to support the terminal differentiation of NSCs towards fully mature neurons. It is noteworthy that here CeO_2 nanoparticles were physically attached to the hydrogels, thus possibly preventing their cellular internalization and possible detrimental effects on the neuronal lineage differentiation of the seeded NSCs, as it has been suggested in other studies.[90] Moreover, in accordance with our study, CeO_2 nanoparticles have also been shown to protect cells against oxidative stress, improving neuronal function and delaying neuronal death after a traumatic brain injury both *in vitro* and *in vivo*.[91]

As previously stated, a glial and neuronal equilibrium is primordial for cell survival and functionality of nerve tissues.[11] Herein, in the absence of CeO_2 nanoparticles (GO : AsA 1 : 1 and 1 : 4 hydrogels), the larger pores and lower stiffness and electrical conductivity of the GO : AsA 1 : 1 hydrogel enhanced the generation of neuronal lineage cells with respect to the smaller pores and greater mechanical and electrical properties of the GO : AsA 1 : 4, where there is a preferred differentiation towards glial lineages at shorter periods (Fig. 5D). But, remarkably, at DIV21, in both hydrogels, GO : AsA 1 : 1 and GO : AsA 1 : 4, astrocytes were the major persisting cell type, despite the detection of some populations of neuronal lineage cells at shorter time points, DIV7 and DIV14. This result comes in agreement with the fact that astrocytes are the metabolically most resistant (least demanding) cell type of the CNS, whose high endogenous antioxidant and glycolytic capacity endows them with a higher ability to survive in adverse conditions.[83,92,93] It is very likely that most of the DCX+ and MAP2+ neuronal cells that were being generated in the GO : AsA 1 : 1 hydrogel at DIV7 and DIV14 eventually perished at DIV21, because of an insufficient antioxidant capacity to support the increased mitochondrial oxidative phosphorylation that comes along with mature neuronal differentiation.[94] Interestingly, in the presence of CeO_2 nanoparticles, the GO : AsA 1 : 4 + CeO_2 0.25 hydrogel supported the co-generation of both MAP2 positive mature neuronal lineage cells together with Olig2 positive oligodendroglial lineage cells until DIV21. The results of this work clearly encourage the incorporation of neuroprotective and antioxidant systems like CeO_2 nanoparticles trapped in tissue engineering scaffolds to boost survival of these two extremely necessary and highly vulnerable cell types of the CNS. The balanced generation of neurons, astrocytes and oligodendrocytes within the bioengineered construct is fundamental for an eventual success of CNS regeneration therapies. It should be emphasized that once a balanced oligodendrocytes, neurons and astrocytes population has been established within the graft, the close contact of the three different cell types may protect each other and improve xenocell survival prior to the integration into the host tissue.[95,96] Indeed, several studies highlighted the necessary integrin mediated connexion between neuronal axons and oligodendrocytes for the survival of both neuronal and oligodendroglial cells *in vitro*.[97,98] Moreover, oligodendrocytes have also been shown to be a glial cell subpopulation that play a key role on axonal regeneration,[98,99] hence the importance of preserving both neurons and oligodendrocytes together in the same bioengineered construct. Here we present a 3D hydrogel based on graphene derivatives and cerium oxide nanoparticles as a promising therapeutic tool for neurodegenerative and demyelinating pathologies involving neuronal and/or oligodendroglial cell death.

Overall, our results showed that hydrogels based on graphene-derivatives supported both glial and neuronal lineage

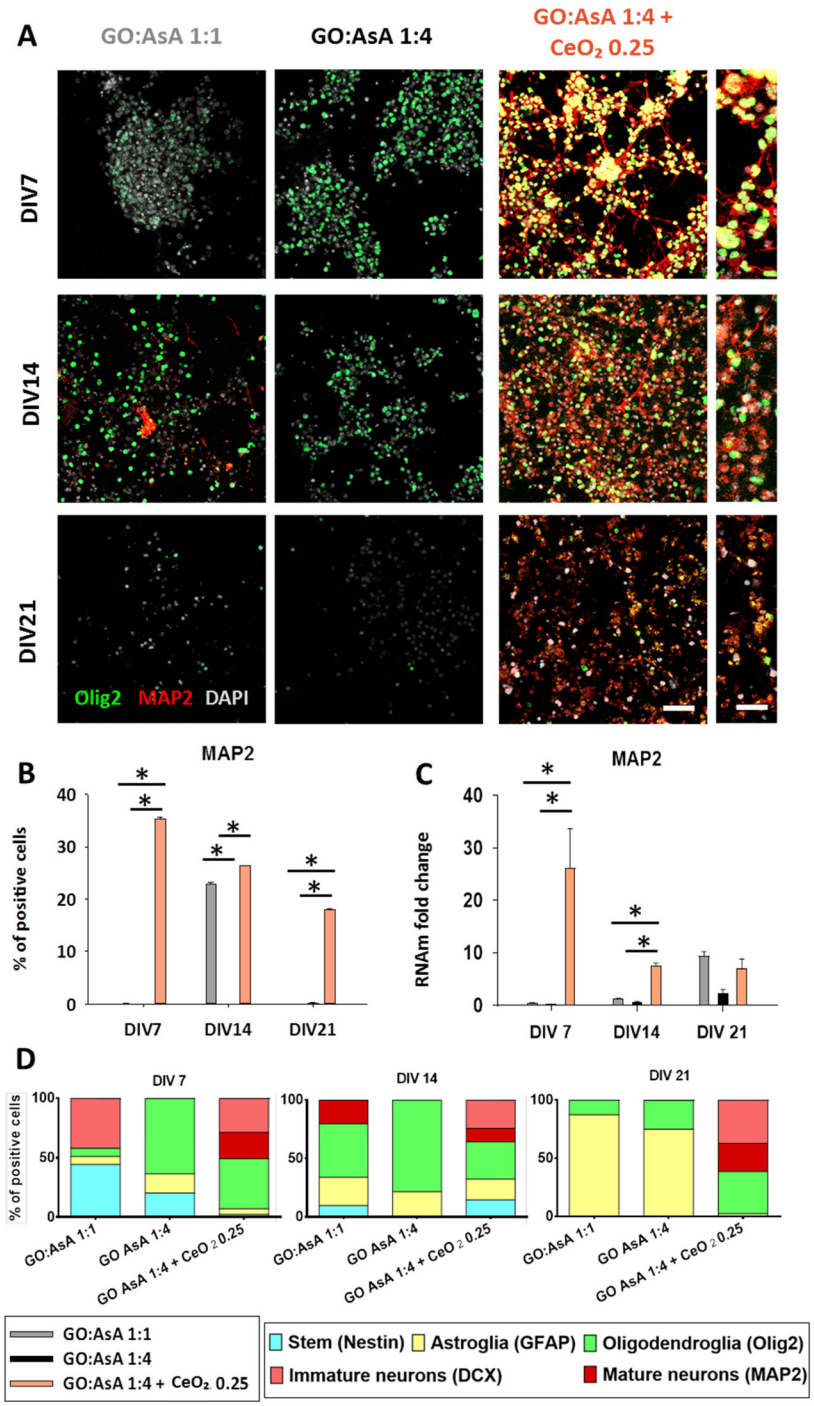

Fig. 5 Generation of *in vitro* co-cultures of neuronal and oligodendroglial lineage cells. (A) Double immunofluorescence showing oligodendroglial Olig2 (green) positive cells together with neuronal MAP2 (red) positive cells in GO : AsA 1 : 1, GO : AsA 1 : 4 and GO : AsA 1 : 4 + CeO_2 0.25 hydrogels after DIV 7, 14 and 21. Scale bar 50 μm. Scale bar of the insets 20 μm. (B) Quantification of the percentage of MAP2 positive cells. (C) qPCR measurements showing the fold change compared to GO : AsA 1 : 1 hydrogel at DIV7. (*$p < 0.05$ compared to the other hydrogels at the same time-points. Holm–Šídák method One-way ANOVA Analysis of Variance on Ranks) (D) Relative proportions of each of the cell lineages in the hydrogels over time. Neural stem (Nestin positive), astroglial (GFAP positive cells), oligodendroglial (Olig2 positive cells), immature neuronal (DCX positive), mature neuronal (MAP2 positive).

differentiation of NSCs in short-term cultures. Softer substrates like GO : AsA 1 : 1 with larger pores and lower electrical conductivities promoted cell differentiation towards neuronal lineages, while stiffer substrates like GO : AsA 1 : 4 with smaller pores and greater electrical properties enhanced glial cell differentiation. However, for long-term cultures, graphene derivatives-based

hydrogels alone were unable to sustain a balanced long-term survival of neurons and oligodendrocytes. In contrast, thanks to the antioxidant and neuroprotective capabilities of CeO_2 nanoparticles embedded on GO : AsA 1 : 4 + CeO_2 0.25, this hydrogel was able to support the generation of astroglial, oligodendroglial and neuronal cells until DIV21, providing a promising approach for CNS regeneration therapies.

4. Conclusions

Herein, we present a simple and scalable method to fabricate 3D hydrogels based on graphene derivatives and CeO_2 nanoparticles promoted by a self-assembly process. The resulting hydrogels showed highly porous structures with tunable electrical, morphological and mechanical properties that can be finely regulated by the addition of AsA and CeO_2 nanoparticles. The final properties of the scaffolds, together with the advanced functionalities provided by the CeO_2 nanoparticles, clearly determined the fate of NSCs, which were seeded on the hydrogels without any ECM-like compound coating or FBS supplementation. Accordingly, we found that softer hydrogels with larger pores and lower electrical conductivity (*i.e.*, GO : AsA 1 : 1) induced an increase of neuronal lineage differentiation, whereas the stiffer ones with smaller pores and greater electrical properties (*i.e.*, GO : AsA 1 : 4) promoted glial cell lineage differentiation. Remarkably, the hydrogel containing CeO_2 nanoparticles (*i.e.*, GO : AsA 1 : 4 + CeO_2 0.25) was the only one allowing the long-term establishment of a mature co-culture containing abundant populations of both neuronal and oligodendroglial lineage cells, which are the two most delicate and difficult to sustain cell types of the CNS. Our findings provide valuable insight on the creation and optimization of differentiated glial and neuronal 3D co-culture systems that enable the integration of both neurons and oligodendrocytes in a same hydrogel scaffold, which could be very useful for future CNS regeneration therapies.

Author contributions

Y.P.: conceptualization, investigation, writing – original draft; J.L.: investigation, writing – review & editing; S.G.L.: investigation; B.P.R.: investigation; D.E.M.T.: investigation; C.T.: investigation; I.M.R.: investigation; E.M.: investigation; J.M.U.: investigation; G.C.: investigation, supervision; G.I.: conceptualization, writing – review & editing, funding acquisition; F.U.: funding acquisition; J.R.S.: conceptualization, funding acquisition, supervision; J.R.P.: conceptualization, investigation, writing – review & editing, supervision, funding acquisition; A. L.: conceptualization, investigation, writing – review & editing, supervision, funding acquisition.

Conflicts of interest

There are no conflicts of interest to declare.

Acknowledgements

We would like to thank Jorge Fernandez (Polimerbio SL) for the support in this project. SGIker technical services (UPV/EHU) are gratefully acknowledged for XPS, XRD, SEM and TEM support. We would like to thank Ricardo Andrade and Alejandro Díez, responsible of the High-Resolution Analytical Microscopy Service in Biomedicine (SGIker UPV/EHU), for their invaluable help for the electron microscopy and cell videorecording assistance. We would like to thank Laura Escobar for confocal microscopy in the Achucarro Basque Center for Neuroscience Fundazioa and Fabrice Cordelières (Bordeaux Imaging Center) for the macro developed for ImageJ.

This work has been funded by the Basque Government (GV/EJ) Department of Education (GIC21/131 IT1766-22, IT1751-22), Health Department (RIS3, 2021333012), Grants PID2019-106236GB-I00 and PID2019-104766RB-C21 funded by MCIN/AEI/10.13039/501100011033. Grant RYC-2013-13450 funded by MCIN/AEI/10.13039/501100011033 and by "ESF investing in your future" by the "European Union" and Achucarro Seed-Fund 003 (JRP), the University of the Basque Country (UPV/EHU) by GIU19/040, GIU 20/050, PPGA 20/22, COLAB19/03 and IKERTU-2020.0155. GV/EJ, Hazitek ZE-2019/00012-IMABI and ELKARTEK KK-2019/00093. Polimerbio and Y. P. have a Bikaintek PhD grant (20-AFW2-2018-00001). Part of this research was performed within the framework of the European Union's Horizon 2020 research and innovation program under the Marie Skłodowska-Curie Grant Agreement No. 793644 (BIONICS).

References

1 V. L. Feigin, A. A. Abajobir, K. H. Abate, F. Abd-Allah, A. M. Abdulle, S. F. Abera, G. Y. Abyu, M. B. Ahmed, A. N. Aichour, I. Aichour, M. T. E. Aichour, R. O. Akinyemi, S. Alabed, R. Al-Raddadi, N. Alvis-Guzman, A. T. Amare, H. Ansari, P. Anwari, J. Ärnlöv, H. Asayesh, S. W. Asgedom, T. M. Atey, L. Avila-Burgos, E. Frinel, G. A. Avokpaho, M. R. Azarpazhooh, A. Barac, M. Barboza, S. L. Barker-Collo, T. Bärnighausen, N. Bedi, E. Beghi, D. A. Bennett, I. M. Bensenor, A. Berhane, B. D. Betsu, S. Bhaumik, S. M. Birlik, S. Biryukov, D. J. Boneya, L. N. B. Bulto, H. Carabin, D. Casey, C. A. Castañeda-Orjuela, F. Catalá-López, H. Chen, A. A. Chitheer, R. Chowdhury, H. Christensen, L. Dandona, R. Dandona, G. A. de Veber, S. D. Dharmaratne, H. P. Do, K. Dokova, E. R. Dorsey, R. G. Ellenbogen, S. Eskandarieh, M. S. Farvid, S.-M. Fereshtehnejad, F. Fischer, K. J. Foreman, J. M. Geleijnse, R. F. Gillum, G. Giussani, E. M. Goldberg, P. N. Gona, A. C. Goulart, H. C. Gugnani, R. Gupta, V. Hachinski, R. Gupta, R. R. Hamadeh, M. Hambisa, G. J. Hankey, H. A. Hareri, R. Havmoeller, S. I. Hay, P. Heydarpour, P. J. Hotez, M. B. Jakovljevic, M. Javanbakht, P. Jeemon, J. B. Jonas, Y. Kalkonde,

A. Kandel, A. Karch, A. Kasaeian, A. Kastor, P. N. Keiyoro, Y. S. Khader, I. A. Khalil, E. A. Khan, Y.-H. Khang, A. Tawfih, A. Khoja, J. Khubchandani, C. Kulkarni, D. Kim, Y. J. Kim, M. Kivimaki, Y. Kokubo, S. Kosen, M. Kravchenko, R. V. Krishnamurthi, B. K. Defo, G. A. Kumar, R. Kumar, H. H. Kyu, A. Larsson, P. M. Lavados, Y. Li, X. Liang, M. L. Liben, W. D. Lo, G. Logroscino, P. A. Lotufo, C. T. Loy, M. T. Mackay, H. M. A. E. Razek, M. M. A. E. Razek, A. Majeed, R. Malekzadeh, T. Manhertz, L. G. Mantovani, J. Massano, M. Mazidi, C. McAlinden, S. Mehata, M. M. Mehndiratta, Z. A. Memish, W. Mendoza, M. A. Mengistie, G. A. Mensah, A. Meretoja, H. B. Mezgebe, T. R. Miller, S. R. Mishra, N. M. Ibrahim, A. Mohammadi, K. E. Mohammed, S. Mohammed, A. H. Mokdad, M. Moradi-Lakeh, I. M. Velasquez, K. I. Musa, M. Naghavi, J. W. Ngunjiri, C. T. Nguyen, G. Nguyen, Q. L. Nguyen, T. H. Nguyen, E. Nichols, D. N. A. Ningrum, V. M. Nong, B. Norrving, J. J. N. Noubiap, F. A. Ogbo, M. O. Owolabi, J. D. Pandian, P. G. Parmar, D. M. Pereira, M. Petzold, M. R. Phillips, M. A. Piradov, R. G. Poulton, F. Pourmalek, M. Qorbani, A. Rafay, M. Rahman, M. H. Rahman, R. K. Rai, S. Rajsic, A. Ranta, S. Rawaf, A. M. N. Renzaho, M. S. Rezai, G. A. Roth, G. Roshandel, E. Rubagotti, P. Sachdev, S. Safiri, R. Sahathevan, M. A. Sahraian, A. M. Samy, P. Santalucia, I. S. Santos, B. Sartorius, M. Satpathy, M. Sawhney, M. I. Saylan, S. G. Sepanlou, M. A. Shaikh, R. Shakir, M. Shamsizadeh, K. N. Sheth, M. Shigematsu, H. Shoman, D. A. S. Silva, M. Smith, E. Sobngwi, L. A. Sposato, J. D. Stanaway, D. J. Stein, T. J. Steiner, L. J. Stovner, R. S. Abdulkader, C. E. Szoeke, R. Tabarés-Seisdedos, D. Tanne, A. M. Theadom, A. G. Thrift, D. L. Tirschwell, R. Topor-Madry, B. X. Tran, T. Truelsen, K. B. Tuem, K. N. Ukwaja, O. A. Uthman, Y. Y. Varakin, T. Vasankari, N. Venketasubramanian, V. V. Vlassov, F. Wadilo, T. Wakayo, M. T. Wallin, E. Weiderpass, R. Westerman, T. Wijeratne, C. S. Wiysonge, M. A. Woldu, C. D. A. Wolfe, D. Xavier, G. Xu, Y. Yano, H. H. Yimam, N. Yonemoto, C. Yu, Z. Zaidi, M. E. S. Zaki, J. R. Zunt, C. J. L. Murray and T. Vos, *Lancet Neurol.*, 2017, **16**, 877–897.

2 World Health Organization - Neurological disorders public health challenges.pdf, (n.d.). **https://www.who.int/mental_health/neurology/neurological_disorders_report_web.pdf** (accessed July 2, 2021).

3 P. M. Rossini, C. Calautti, F. Pauri and J.-C. Baron, *Lancet Neurol.*, 2003, **2**, 493–502.

4 I. Fischer, J. N. Dulin and M. A. Lane, *Nat. Rev. Neurosci.*, 2020, **21**, 366–383.

5 X. Tian, T. Fan, W. Zhao, G. Abbas, B. Han, K. Zhang, N. Li, N. Liu, W. Liang, H. Huang, W. Chen, B. Wang and Z. Xie, *Bioact. Mater.*, 2021, **6**, 2854–2869.

6 S. Jarrin, S. Cabré and E. Dowd, *Neurochem. Int.*, 2021, **144**, 104971.

7 S. Grade and M. Götz, *npj Regener. Med.*, 2017, **2**, 1–11.

8 Y. Li, Y. Xiao and C. Liu, *Chem. Rev.*, 2017, **117**, 4376–4421.

9 R. Kumar, R. Rauti, D. Scaini, M. Antman-Passig, O. Meshulam, D. Naveh, L. Ballerini and O. Shefi, *Adv. Funct. Mater.*, 2021, **31**, 2104887.

10 A. Capasso, J. Rodrigues, M. Moschetta, F. Buonocore, G. Faggio, G. Messina, M. J. Kim, J. Kwon, E. Placidi, F. Benfenati, M. Bramini, G.-H. Lee and N. Lisi, *Adv. Funct. Mater.*, 2021, **31**, 2005300.

11 Y. Polo, J. Luzuriaga, J. Iturri, I. Irastorza, J. L. Toca-Herrera, G. Ibarretxe, F. Unda, J.-R. Sarasua, J. R. Pineda and A. Larrañaga, *Nanomedicine*, 2021, **31**, 102314.

12 C. Tapeinos, *Adv. NanoBiomed Res.*, 2021, **1**, 2000059.

13 Q. Ma, L. Yang, Z. Jiang, Q. Song, M. Xiao, D. Zhang, X. Ma, T. Wen and G. Cheng, *ACS Appl. Mater. Interfaces*, 2016, **8**, 34227–34233.

14 Q. Fang, Y. Zhang, X. Chen, H. Li, L. Cheng, W. Zhu, Z. Zhang, M. Tang, W. Liu, H. Wang, T. Wang, T. Shen and R. Chai, *Front. Bioeng. Biotechnol.*, 2020, **7**, 436.

15 N. Sultana, M. I. Hassan and M. M. Lim, *Composite Synthetic Scaffolds for Tissue Engineering and Regenerative Medicine*, Springer International Publishing, Cham, 2015.

16 K. R. Singh, V. Nayak, T. Sarkar and R. P. Singh, *RSC Adv.*, 2020, **10**, 27194–27214.

17 C. Xu and X. Qu, *NPG Asia Mater.*, 2014, **6**, e90–e90.

18 Y. Qian, Q. Han, X. Zhao, H. Li, W.-E. Yuan and C. Fan, *iScience*, 2019, **12**, 216–231.

19 M. Das, S. Patil, N. Bhargava, J.-F. Kang, L. M. Riedel, S. Seal and J. J. Hickman, *Biomaterials*, 2007, **28**, 1918–1925.

20 A. Ranjbar, S. Soleimani Asl, F. Firozian, H. Heidary Dartoti, S. Seyedabadi, M. Taheri Azandariani and M. Ganji, *J. Mol. Neurosci.*, 2018, **66**, 420–427.

21 K. J. Livak and T. D. Schmittgen, *Methods*, 2001, **25**, 402–408.

22 S. Pei and H.-M. Cheng, *Carbon*, 2012, **50**, 3210–3228.

23 V. Agarwal and P. B. Zetterlund, *Chem. Eng. J.*, 2021, **405**, 127018.

24 Y. Shang, D. Zhang, Y. Liu and C. Guo, *Bull. Mater. Sci.*, 2015, **38**, 7–12.

25 C. K. Chua and M. Pumera, *Chem. Soc. Rev.*, 2013, **43**, 291–312.

26 N. Ormategui, A. Veloso, G. P. Leal, S. Rodriguez-Couto and R. Tomovska, *ACS Appl. Mater. Interfaces*, 2015, **7**, 14104–14112.

27 K. K. H. De Silva, H.-H. Huang and M. Yoshimura, *Appl. Surf. Sci.*, 2018, **447**, 338–346.

28 O. C. Compton and S. T. Nguyen, *Small*, 2010, **6**, 711–723.

29 Y. Xu, K. Sheng, C. Li and G. Shi, *ACS Nano*, 2010, **4**, 4324–4330.

30 E. Nicolas, S. Callé, S. Nicolle, D. Mitton and J.-P. Remenieras, *Ultrasonics*, 2018, **84**, 119–125.

31 S. Cheng, E. C. Clarke and L. E. Bilston, *Med. Eng. Phys.*, 2008, **30**, 1318–1337.

32 Z. Ma, S. Hu, J. S. Tan, C. Myer, N. M. Njus and Z. Xia, *J. Biomed. Mater. Res., Part A*, 2013, **101**, 2718–2725.

33 A. F. Girão, J. Sousa, A. Domínguez-Bajo, A. González-Mayorga, I. Bdikin, E. Pujades-Otero, N. Casañ-Pastor, M. J. Hortigüela, G. Otero-Irurueta, A. Completo, M. C. Serrano and P. A. A. P. Marques, *ACS Appl. Mater. Interfaces*, 2020, **12**, 38962–38975.
34 S. Chae, T.-H. Le, C. S. Park, Y. Choi, S. Kim, U. Lee, E. Heo, H. Lee, Y. A. Kim, O. S. Kwon and H. Yoon, *Nanoscale*, 2020, **12**, 13351–13359.
35 S. Rao, J. Upadhyay, K. Polychronopoulou, R. Umer and R. Das, *J. Compos. Sci.*, 2018, **2**, 25.
36 Z. Tan, S. Ohara, H. Abe and M. Naito, *RSC Adv.*, 2014, **4**, 8874–8878.
37 X. Jing, H.-Y. Mi, B. N. Napiwocki, X.-F. Peng and L.-S. Turng, *Carbon*, 2017, **125**, 557–570.
38 J. Park, J. H. Choi, S. Kim, I. Jang, S. Jeong and J. Y. Lee, *Acta Biomater.*, 2019, **97**, 141–153.
39 J. E. Hirsch, *Phys. C*, 1992, **199**, 305–310.
40 Y. Nioua, S. El Bouazzaoui, B. M. G. Melo, P. R. S. Prezas, M. P. F. Graça, M. E. Achour, L. C. Costa and C. Brosseau, *J. Mater. Sci.*, 2017, **52**, 13790–13798.
41 L. Koessler, S. Colnat-Coulbois, T. Cecchin, J. Hofmanis, J. P. Dmochowski, A. M. Norcia and L. G. Maillard, *Hum. Brain Mapp.*, 2017, **38**, 974–986.
42 H. McCann, G. Pisano and L. Beltrachini, *Brain Topogr.*, 2019, **32**, 825–858.
43 P. Zarrintaj, S. Manouchehri, Z. Ahmadi, M. R. Saeb, A. M. Urbanska, D. L. Kaplan and M. Mozafari, *Carbohydr. Polym.*, 2018, **187**, 66–84.
44 A. Saberi, F. Jabbari, P. Zarrintaj, M. R. Saeb and M. Mozafari, *Biomolecules*, 2019, **9**, 448.
45 A. Y. Estevez and J. S. Erlichman, *Nanomedicine*, 2014, **9**, 1437–1440.
46 J. Cui and G. A. Hope, *J. Spectrosc.*, 2015, **2015**, e940172.
47 J.-B. Wu, M.-L. Lin, X. Cong, H.-N. Liu and P.-H. Tan, *Chem. Soc. Rev.*, 2018, **47**, 1822–1873.
48 B. Gupta, N. Kumar, K. Panda, V. Kanan, S. Joshi and I. Visoly-Fisher, *Sci. Rep.*, 2017, **7**, 45030.
49 Y. Yang, C. Tian, L. Sun, R. Lü, W. Zhou, K. Shi, K. Kan, J. Wang and H. Fu, *J. Mater. Chem. A*, 2013, **1**, 12742.
50 Y. Si and E. T. Samulski, *Chem. Mater.*, 2008, **20**, 6792–6797.
51 S. M. Hirst, A. S. Karakoti, R. D. Tyler, N. Sriranganathan, S. Seal and C. M. Reilly, *Small*, 2009, **5**, 2848–2856.
52 G. Song, N. Cheng, J. Zhang, H. Huang, Y. Yuan, X. He, Y. Luo and K. Huang, *Catalysts*, 2021, **11**, 1123.
53 C. Korsvik, S. Patil, S. Seal and W. T. Self, *Chem. Commun.*, 2007, 1056–1058.
54 S. M. Hirst, A. Karakoti, S. Singh, W. Self, R. Tyler, S. Seal and C. M. Reilly, *Environ. Toxicol.*, 2013, **28**, 107–118.
55 H. Sies, *Redox Biol.*, 2017, **11**, 613–619.
56 G. Ciofani, G. G. Genchi, I. Liakos, V. Cappello, M. Gemmi, A. Athanassiou, B. Mazzolai and V. Mattoli, *Pharm. Res.*, 2013, **30**, 2133–2145.
57 J. Yi, G. Choe, J. Park and J. Y. Lee, *Polym. J.*, 2020, **52**, 823–837.
58 J. D. Lathia, M. Li, P. E. Hall, J. Gallagher, J. S. Hale, Q. Wu, M. Venere, E. Levy, M. R. S. Rani, P. Huang, E. Bae, J. Selfridge, L. Cheng, H. Guvenc, R. E. McLendon, I. Nakano, A. E. Sloan, H. S. Phillips, A. Lai, C. L. Gladson, M. Bredel, S. Bao, A. B. Hjelmeland and J. N. Rich, *Ann. Neurol.*, 2012, **72**, 766–778.
59 C. A. Gregory, E. Reyes, M. J. Whitney and J. L. Spees, *Stem Cells*, 2006, **24**, 2232–2243.
60 U. Lendahl, L. B. Zimmerman and R. D. McKay, *Cell*, 1990, **60**, 585–595.
61 S. Suzuki, J. Namiki, S. Shibata, Y. Mastuzaki and H. Okano, *J. Histochem. Cytochem.*, 2010, **58**, 721–730.
62 A. Bernal and L. Arranz, *Cell. Mol. Life Sci.*, 2018, **75**, 2177–2195.
63 J. Dahlstrand, M. Lardelli and U. Lendahl, *Brain Res. Dev. Brain Res.*, 1995, **84**, 109–129.
64 F. Doetsch, J. M. García-Verdugo and A. Alvarez-Buylla, *J. Neurosci.*, 1997, **17**, 5046–5061.
65 S. Shaban, M. W. A. El-Husseny, A. I. Abushouk, A. M. A. Salem, M. Mamdouh and M. M. Abdel-Daim, *Oxid. Med. Cell. Longevity*, 2017, **2017**, 5032102.
66 J. Lugrin, N. Rosenblatt-Velin, R. Parapanov and L. Liaudet, *Biol. Chem.*, 2014, **395**, 203–230.
67 C. T. Ekdahl, J.-H. Claasen, S. Bonde, Z. Kokaia and O. Lindvall, *Proc. Natl. Acad. Sci. U. S. A.*, 2003, **100**, 13632–13637.
68 L. Ottoboni, B. von Wunster and G. Martino, *Front. Neurol.*, 2020, **11**, 148.
69 F. H. Gage and S. Temple, *Neuron*, 2013, **80**, 588–601.
70 K. H. Lee, M. Cha and B. H. Lee, *Int. J. Mol. Sci.*, 2021, **22**, 13315.
71 Q. Ma, L. Yang, Z. Jiang, Q. Song, M. Xiao, D. Zhang, X. Ma, T. Wen and G. Cheng, *ACS Appl. Mater. Interfaces*, 2016, **8**, 34227–34233.
72 K. Saha, A. J. Keung, E. F. Irwin, Y. Li, L. Little, D. V. Schaffer and K. E. Healy, *Biophys. J.*, 2008, **95**, 4426–4438.
73 S. Sergent-Tanguy, D. C. Michel, I. Neveu and P. Naveilhan, *J. Neurosci. Res.*, 2006, **83**, 1515–1524.
74 D. C. Lagace, M. C. Whitman, M. A. Noonan, J. L. Ables, N. A. DeCarolis, A. A. Arguello, M. H. Donovan, S. J. Fischer, L. A. Farnbauch, R. D. Beech, R. J. DiLeone, C. A. Greer, C. D. Mandyam and A. J. Eisch, *J. Neurosci.*, 2007, **27**, 12623–12629.
75 M. V. Sofroniew and H. V. Vinters, *Acta Neuropathol.*, 2010, **119**, 7–35.
76 H. Kawano, J. Kimura-Kuroda, Y. Komuta, N. Yoshioka, H. P. Li, K. Kawamura, Y. Li and G. Raisman, *Cell Tissue Res.*, 2012, **349**, 169–180.
77 A. McKeon and E. E. Benarroch, *Neurology*, 2018, **90**, 925–930.
78 E. Raponi, F. Agenes, C. Delphin, N. Assard, J. Baudier, C. Legraverend and J.-C. Deloulme, *Glia*, 2007, **55**, 165–177.
79 J. R. Pineda, M. Daynac, A. Chicheportiche, A. Cebrian-Silla, K. Sii Felice, J. M. Garcia-Verdugo, F. D. Boussin and M.-A. Mouthon, *EMBO Mol. Med.*, 2013, **5**, 548–562.

80 G. Santos, A. Barateiro, D. Brites and A. Fernandes, *Front. Cell. Neurosci.*, 2020, **14**, 279.
81 A. Wegener, C. Deboux, C. Bachelin, M. Frah, C. Kerninon, D. Seilhean, M. Weider, M. Wegner and B. Nait-Oumesmar, *Brain J. Neurol.*, 2015, **138**, 120–135.
82 G. Ibarretxe, M. V. Sánchez-Gómez, M. R. Campos-Esparza, E. Alberdi and C. Matute, *Glia*, 2006, **53**, 201–211.
83 S. K. Thorburne and B. H. J. Juurlink, *J. Neurochem.*, 1996, **67**, 1014–1022.
84 E. Eitan, E. R. Hutchison, N. H. Greig, D. Tweedie, H. Celik, S. Ghosh, K. W. Fishbein, R. G. Spencer, C. Y. Sasaki, P. Ghosh, S. Das, S. Chigurapati, J. Raymick, S. Sarkar, S. Chigurupati, S. Seal and M. P. Mattson, *Exp. Neurol.*, 2015, **273**, 151–160.
85 N. Pirotte, N. Leynen, T. Artois and K. Smeets, *Dev. Biol.*, 2016, **409**, 4–15.
86 M. E. van Strien, S. A. van den Berge and E. M. Hol, *Cell Res.*, 2011, **21**, 1523–1525.
87 T. L. Walker, T. Yasuda, D. J. Adams and P. F. Bartlett, *J. Neurosci.*, 2007, **27**, 3734–3742.
88 T. Kremer, R. Jagasia, A. Herrmann, H. Matile, E. Borroni, F. Francis, H. G. Kuhn and C. Czech, *PLoS One*, 2013, **8**, e59269.
89 J. G. Izant and J. R. McIntosh, *Proc. Natl. Acad. Sci. U. S. A.*, 1980, **77**, 4741–4745.
90 A. R. Gliga, K. Edoff, F. Caputo, T. Källman, H. Blom, H. L. Karlsson, L. Ghibelli, E. Traversa, S. Ceccatelli and B. Fadeel, *Sci. Rep.*, 2017, **7**, 9284.
91 Z. S. Bailey, E. Nilson, J. A. Bates, A. Oyalowo, K. S. Hockey, V. S. S. S. Sajja, C. Thorpe, H. Rogers, B. Dunn, A. S. Frey, M. J. Billings, C. A. Sholar, A. Hermundstad, C. Kumar, P. J. VandeVord and B. A. Rzigalinski, *J. Neurotrauma*, 2020, **37**, 1452–1462.
92 B. H. J. Juurlink, S. K. Thorburne and L. Hertz, *Glia*, 1998, **22**, 371–378.
93 A. Almeida, J. Almeida, J. P. Bolaños and S. Moncada, *Proc. Natl. Acad. Sci. U. S. A.*, 2001, **98**, 15294–15299.
94 C. Maffezzini, J. Calvo-Garrido, A. Wredenberg and C. Freyer, *Cell. Mol. Life Sci.*, 2020, **77**, 2483–2496.
95 M. J. Rigby, T. M. Gomez and L. Puglielli, *Front. Neurosci.*, 2020, **14**, 203.
96 A. Amaral, T. Meisingset, M. Kotter and U. Sonnewald, *Front. Endocrinol.*, 2013, **4**, 54.
97 E. E. Frost, P. C. Buttery, R. Milner and C. ffrench-Constant, *Curr. Biol.*, 1999, **9**, 1251–12S1.
98 L. Gang, Y. Yao, Y. Liu, Y. Li, K. Yang, L. Lu, Y. Cheng, X. Chen and Y. Tu, *Neural Regener. Res.*, 2015, **10**, 1612–1616.
99 K. A. Chamberlain, S. E. Nanescu, K. Psachoulia and J. K. Huang, *Neuropharmacology*, 2016, **110**, 633–643.